

A STUDY OF THE REACTIONS
 $^{149,151}\text{Sm}(p,t)^{147,149}\text{Sm}$

A STUDY OF THE REACTIONS
 $^{149,151}\text{Sm}(p,t)^{147,149}\text{Sm}$

by

ROBERT DAVID GADSBY, B.Sc.

A Thesis

Submitted to the Faculty of Graduate Studies

in Partial Fulfilment of the Requirements

for the Degree

Master of Science

McMaster University

September 1972

MASTER OF SCIENCE
(Physics)

McMASTER UNIVERSITY
Hamilton, Ontario

TITLE: A Study of the Reactions $^{149,151}\text{Sm}(p,t)^{147,149}\text{Sm}$

AUTHOR: Robert David Gadsby, B.Sc. (McMaster University)

SUPERVISOR: Dr. D.G. Burke

NUMBER OF PAGES: vii, 53

SCOPE AND CONTENTS: Two-neutron pick-up reactions have been performed on targets of ^{149}Sm and radioactive ^{151}Sm using 18 MeV protons. The outgoing tritons from the ^{151}Sm target were analyzed with a magnetic spectrograph at 16 angles between 6° and 80° . Unlike the two-neutron transfer data on neighbouring even-even targets, the angular distributions indicated $\ell=0$ transitions to many levels in the final nucleus. Partial angular distributions for the $^{149}\text{Sm}(p,t)^{147}\text{Sm}$ reaction were obtained, but showed only one strong $\ell=0$ transition populating the ^{147}Sm ground state. In addition, spectra from the $^{152}\text{Sm}(p,t)$ reaction were measured at several angles in order to provide normalization to previous results.

ACKNOWLEDGEMENTS

I wish to express my appreciation to Dr. D.G. Burke for his support and guidance. I would also like to thank Dr. J.C. Waddington for his helpful discussions.

I am grateful to the operations personnel of the McMaster Tandem Accelerator for their cooperation during the course of these experiments. Thanks are also due to D.E. Nelson and O.P. Jolly for their help with target construction, T. Taylor for his assistance with the DWUCK program, Mrs. J. Prestwich and Mrs. D. Vince for carefully scanning the nuclear emulsions, Miss J. Balogh for drawing the figures, and Jan Coleman for her speed and accuracy in typing this manuscript.

Financial assistance for this work was provided by the National Research Council of Canada in the form of an operating grant and scholarship support.

TABLE OF CONTENTS

	Page	
CHAPTER I	INTRODUCTION	1
	1.1 A Survey of Previous Work	1
CHAPTER II	THEORETICAL CONSIDERATIONS	6
	2.1 Nuclear Models	6
	2.1.1 Shell Model	6
	2.1.2 Nilsson Model	8
	2.1.3 Optical Model	9
	2.2 Direct Reactions	12
	2.2.1 Two-Nucleon Transfer Reactions	12
CHAPTER III	THE EXPERIMENT	15
	3.1 Experimental Apparatus and Procedure	15
	3.2 Results and Discussion	20
	3.3 Summary	35
APPENDICES		40
	A1 DWBA Calculations	40
	A2 ^{151}Sm Target Construction	48
REFERENCES		52

LIST OF FIGURES

		Page
Fig. 1.1	The low-lying energy levels of ^{150}Sm and ^{152}Sm .	2
Fig. 1.2	The $\ell=0(t,p)$ and (p,t) transitions in the even samarium isotopes.	4
Fig. 2.1	Nilsson diagram for neutron levels in the region $N\approx 90$.	10
Fig. 3.1	Experimental set-up of the target chamber showing the electronics used.	16
Fig. 3.2	Typical trajectories for particles in the Enge split-pole magnetic spectrograph.	18
Fig. 3.3	Triton spectra from the $^{151}\text{Sm}(p,t)^{149}\text{Sm}$ reaction.	22
Fig. 3.4	Angular distributions for $\ell=0$ transitions to levels in ^{149}Sm .	26
Fig. 3.5	Angular distributions for transitions to other levels in ^{149}Sm .	27
Fig. 3.6	Strengths of $\ell=0$ transitions to levels in ^{149}Sm .	29
Fig. 3.7	Triton spectrum from the $^{149}\text{Sm}(p,t)^{147}\text{Sm}$ reaction.	32
Fig. 3.8	The angular distribution of the ground state of ^{147}Sm populated by the $^{149}\text{Sm}(p,t)$ reaction.	33
Fig. 3.9	Angular distributions for $\ell=0$ transitions to levels in ^{150}Sm .	34
Fig. 3.10	The $\ell=0(t,p)$ and (p,t) transitions in the odd samarium isotopes.	37
Fig. A1.1	The effect of various potentials and neutron shells on DWBA $\ell=0$ angular distributions.	42
Fig. A1.2	The effect of changing the beam energy on DWBA $\ell=0$ angular distributions.	44

Fig. A1.3 DWBA predictions of $\ell=2$ and $\ell=4$ angular
distributions for the $1h_{9/2}$ and $2f_{7/2}$ shells.

LIST OF TABLES

		Page
Table 3.1	Isotopic compositions and approximate thickness of the targets.	21
Table 3.2	Cross sections for (p,t) transitions to levels in ^{149}Sm .	23
Table 3.3	Absolute cross sections for selected levels in ^{150}Sm .	30
Table 3.4	Q-values and two-neutron separation energies.	36
Table A1.1	Optical model parameter sets for DWBA calculations.	41

CHAPTER I
INTRODUCTION

1.1 A Survey of Previous Work

Two-nucleon transfer reactions have only recently become a popular method of investigating nuclear structure. The present work makes use of the two-neutron pick-up reaction, (p,t) , to study levels in ^{147}Sm and ^{149}Sm .

In the rare earth region of the periodic table, between neutron numbers $N=88$ and $N=90$, there is an abrupt change from "spherical" (for $N \leq 88$) to "deformed" (for $N \geq 90$) nuclear equilibrium shapes. Evidence of this transition in nuclear deformation may be seen in the low-lying level schemes for even-even nuclei in this region. The level schemes for the low-lying states of the even-even samarium isotopes, ^{150}Sm and ^{152}Sm , are shown in Fig. 1.1 following the compilation of Lederer et al. (1967). The level scheme for ^{150}Sm ($N=88$) shows a triplet with $I^\pi=0^+, 2^+, 4^+$ at about twice the excitation energy of the first excited 2^+ state. This type of energy-level diagram is typical of the 1-phonon and 2-phonon vibrational states of a "spherical" even-even nucleus. On the other hand, a "deformed" even-even nucleus would be expected to have a ground state rotational band, consisting of levels with $I^\pi=0^+, 2^+, 4^+$, etc., whose energies follow the $I(I+1)$ rule. This is, in fact, the case for ^{152}Sm ($N=90$). The $0^+, 2^+, 4^+, 6^+$ sequence in the level scheme has energies which fit approximately the $I(I+1)$ rule. Hence, ^{150}Sm is considered mainly spherical and ^{152}Sm , mainly deformed.

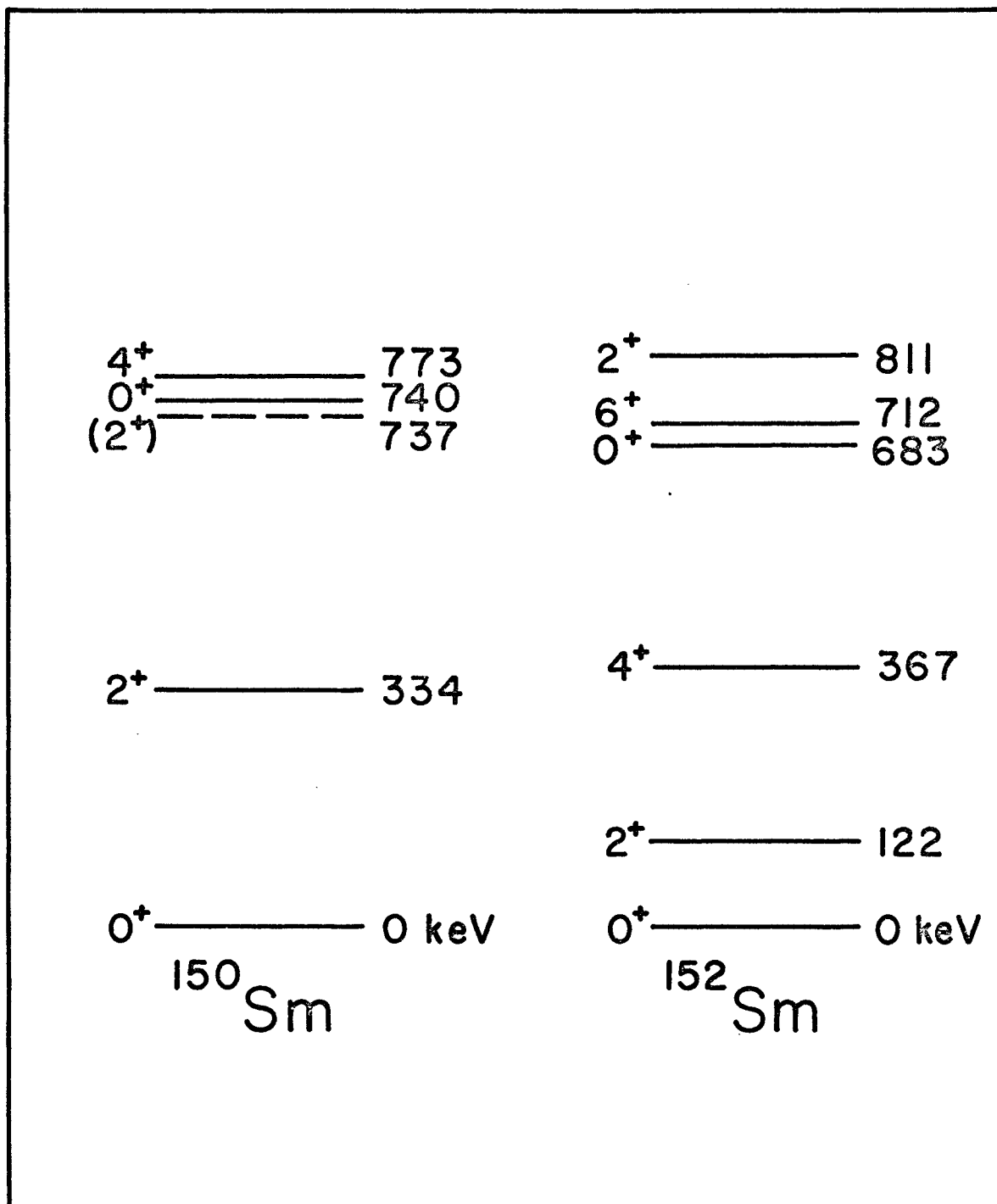


Fig. 1.1 The low-lying energy levels of ^{150}Sm and ^{152}Sm .

A similar transition has been recorded (Lederer et al. 1967) for the low-lying levels of the even-even neodymium and gadolinium nuclei between $N=88$ and $N=90$.

Recently two-neutron transfer reactions on the even isotopes of neodymium, samarium and gadolinium in this region of changing deformation, have been the subject of extensive study. The results of these reactions seem to depend rather dramatically on the shapes of the initial and final nuclei. A summary of the results of (t,p) and (p,t) reactions on the even samarium ($Z=62$) isotopes, as reported by Maxwell et al. (1966), Bjerregaard et al. (1966) and McLatchie et al. (1970) is shown in Fig. 1.2. Only transitions with total angular momentum transfers of zero ($\ell=0$) are shown.

It was discovered that for two-neutron transfer reactions which connected "spherical" nuclei, such as $^{148}\text{Sm}(t,p)^{150}\text{Sm}$, the ground state to ground state transition dominated. In fact, even in the $^{144}\text{Sm}(t,p)$ reaction, where a strong $\ell=0$ transition to an excited 0^+ state in ^{146}Sm was seen, the ground state to ground state transition accounted for about 76% of the total $\ell=0$ strength observed. A similar situation occurred for two-neutron transfer reactions which connected "deformed" nuclei; at least 70% of the total $\ell=0$ strength observed in these reactions appeared in the ground state to ground state transition. However, in the region where there was a change in deformation between the initial

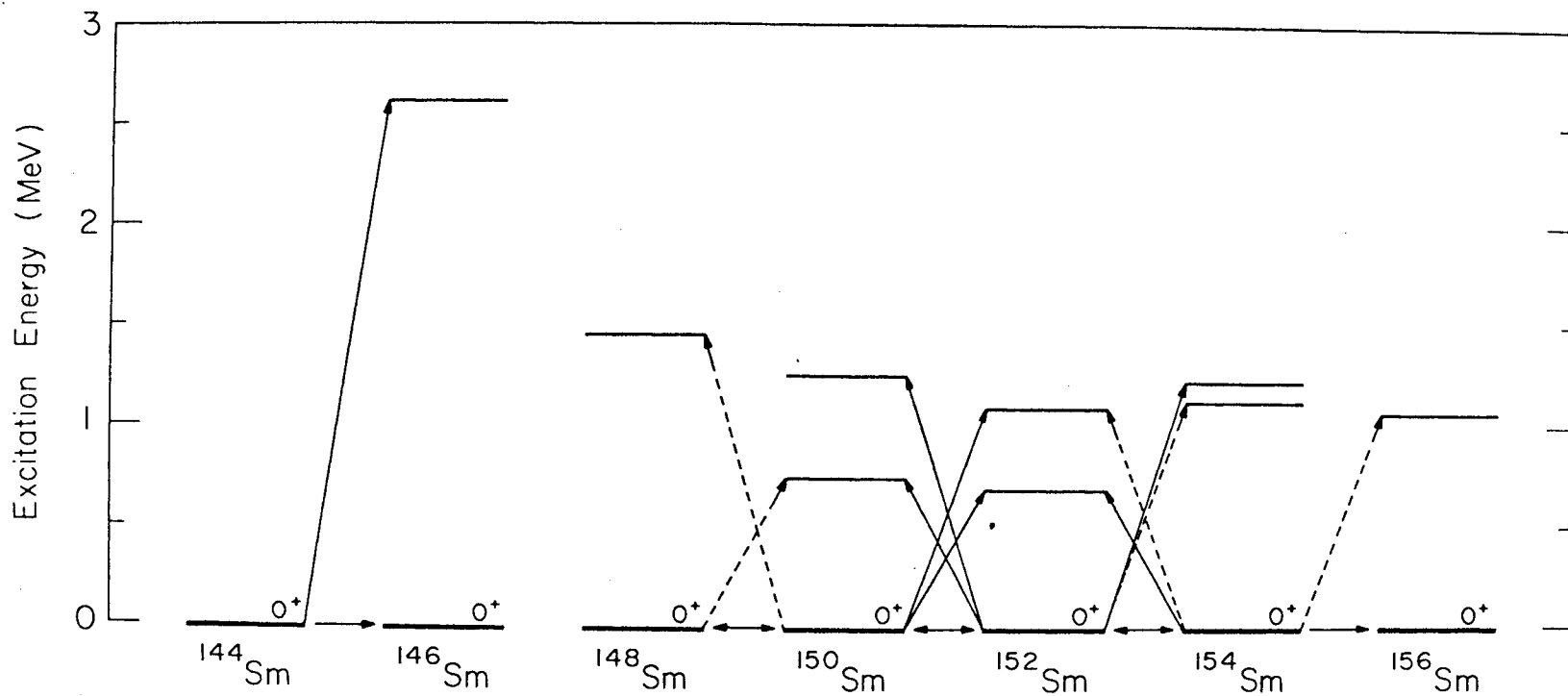


Fig. 1.2 The $\ell=0$ (t,p) and (p,t) transitions in the even samarium isotopes. Arrows pointing to the right indicate (t,p) transitions with $\ell=0$ and those pointing to the left, $\ell=0$ (p,t) transitions. The broken arrows are used for transitions where the strength is less than 25% of the ground state transition.

and final nuclei, an appreciable fraction of the total $\ell=0$ strength appeared in transitions to excited 0^+ states. In the $^{150}\text{Sm}(t,p)$ reaction, the ground state to ground state transition accounted for only 41% of the total $\ell=0$ strength and in the $^{152}\text{Sm}(p,t)$ reaction, only 35%. Similar results for $\ell=0$ transfers have been reported by Fleming et al. (1971) and Elze et al. (1972) from (p,t) studies on the even isotopes of gadolinium and by Chapman et al. (1972) from (t,p) studies on the even isotopes of neodymium. It is apparent from these studies that in a region of changing nuclear deformation it is possible to observe two-neutron transfer reactions, on even-even target nuclei, in which some excited 0^+ states are strongly populated. Usually, however, when there is no significant change in deformation between the initial and final nuclei, only the ground state is strongly populated by this type of reaction. However, as summarized by Elze et al. (1972), other mechanisms also exist for the population of excited 0^+ states.

One further result of the previous studies reported by McLatchie et al. (1970), Chapman et al. (1972) and Elze et al. (1972) was that the shapes of the angular distributions for transitions to excited 2^+ states varied quite drastically. It has been suggested that this may be the result of second order reactions (Brogia et al. 1972), but as yet the situation is not clearly understood.

The present work extends the study of (p,t) reactions to samarium targets with an odd number of neutrons, notably $^{151}\text{Sm}(N=89)$ and $^{149}\text{Sm}(N=87)$.

CHAPTER II

THEORETICAL CONSIDERATIONS

2.1 Nuclear Models

Although no single nuclear model can explain all of the experimentally observed properties of nuclei, several nuclear models are successful in describing particular phenomena or a region of the periodic table. In this section some of the essential characteristics of three nuclear models which are particularly relevant to this work are described. The shell model and Nilsson model are relevant to different regions of the periodic table and the optical model is useful in understanding certain types of nuclear reactions. Detailed descriptions of each of these models may be found in standard nuclear physics textbooks, such as Preston (1962).

2.1.1 Shell Model

Despite the apparent lack of theoretical justification with which the shell model began, this model has been extremely useful in predicting ground state spins, magnetic moments and other properties for spherical nuclei. The development of the model was based on obtaining the "magic numbers", 2, 8, 20, 28, 50, 82, and 126 which were derived from discontinuities in various nuclear trends. In the shell model, each nucleon is assumed to move in a central potential generated by all of the other nucleons and can be described by its own set of quantum numbers. The order of filling of

nuclear levels is governed by the level energy and the Pauli exclusion principle. By the inclusion of $l \cdot s$ coupling, large energy gaps were found to occur, after the filling of appropriate levels, at the "magic numbers". It is in regions of the periodic table near closed shells that the shell model meets with its greatest success.

Shell model predictions of the ground state spins make use of the idea of closed shells. For a closed shell it is assumed that all the spins of the individual nucleons couple to zero. For one particle outside a closed shell the ground state spin, according to this model, is simply the spin of that particle. A similar situation exists for one hole. If two or more nucleons are outside the closed shell the possibilities of pairing and coupling of spins must be considered.

The single-particle model extension of the shell model includes the idea of pairing of the nucleons. Thus pairs of neutrons or protons with their spins antiparallel are placed in the shell model orbits. According to this model extension, the ground state spin of an even-even nucleus is zero since all of the nucleons are paired off. Experimentally it is observed that all even-even nuclei do have ground state spins of zero. For an odd-even nucleus, the ground state spin is assumed to be the spin of the last unpaired nucleon. This is often found experimentally to be

the case for spherical nuclei; for example, for ^{147}Sm and ^{149}Sm , the predicted ground state spin of $7/2$, which results from an unpaired neutron in the $2f_{7/2}$ shell-model state, is in agreement with the experimentally observed value. It is much more difficult to accurately determine the ground state spins of odd-odd nuclei.

The downfall of the shell model has been particularly evident in its prediction of quadrupole moments and transition rates for deformed nuclei. It is, however, possible to use the complete orthogonal set of spherical shell model states as a basis to describe any deformed state. In this way the wavefunction, ψ , of a deformed nuclear state can be expressed as a sum of spherical shell model states, ϕ_i , each having an amplitude, a_i , as follows:

$$\psi = \sum_i a_i \phi_i$$

This development permits the extension of the shell model to deformed states, as outlined in the following section.

2.1.2 Nilsson Model

The observation of large static quadrupole moments in several regions of the periodic table suggested that a deformed rather than spherical potential was required for some nuclei. The potential used in the calculations of Nilsson (1955) was an axially-symmetric oscillator potential with spin-orbit coupling. The single particle wavefunctions were then obtained by solving the Schrödinger equation in

this potential. In order to reproduce the experimental results for strongly deformed nuclei, terms proportional to ℓ^2 and $\ell \cdot s$ were introduced, and the strengths of these terms were adjusted to give the observed shell-model states for zero deformation (spherical nuclei). Fig. 2.1 shows the results of Nilsson model calculations for energies of neutron states in the region $N \approx 90$ as a function of deformation.

Filling of levels in the Nilsson model is accomplished by the filling of neutron and proton levels separately, placing two particles in each state, one with spin up (\uparrow) and the other with spin down (\downarrow), starting with the lowest energy states. This must be done, of course, at the deformation appropriate to the nucleus of interest. The spin predicted in this manner for an odd-N nucleus would simply be that of the last neutron orbital for the unpaired particle. As summarized in a recent report by Bunker and Reich (1971), these predictions are in good agreement with the spins of well deformed nuclei.

2.1.3 Optical Model

The optical model is included in this section since the distorted-wave Born approximation (DWBA) calculations discussed in Appendix A1, were done using optical-model potentials. The model was developed to reproduce the experimental results of particle scattering reactions and has been found to work well

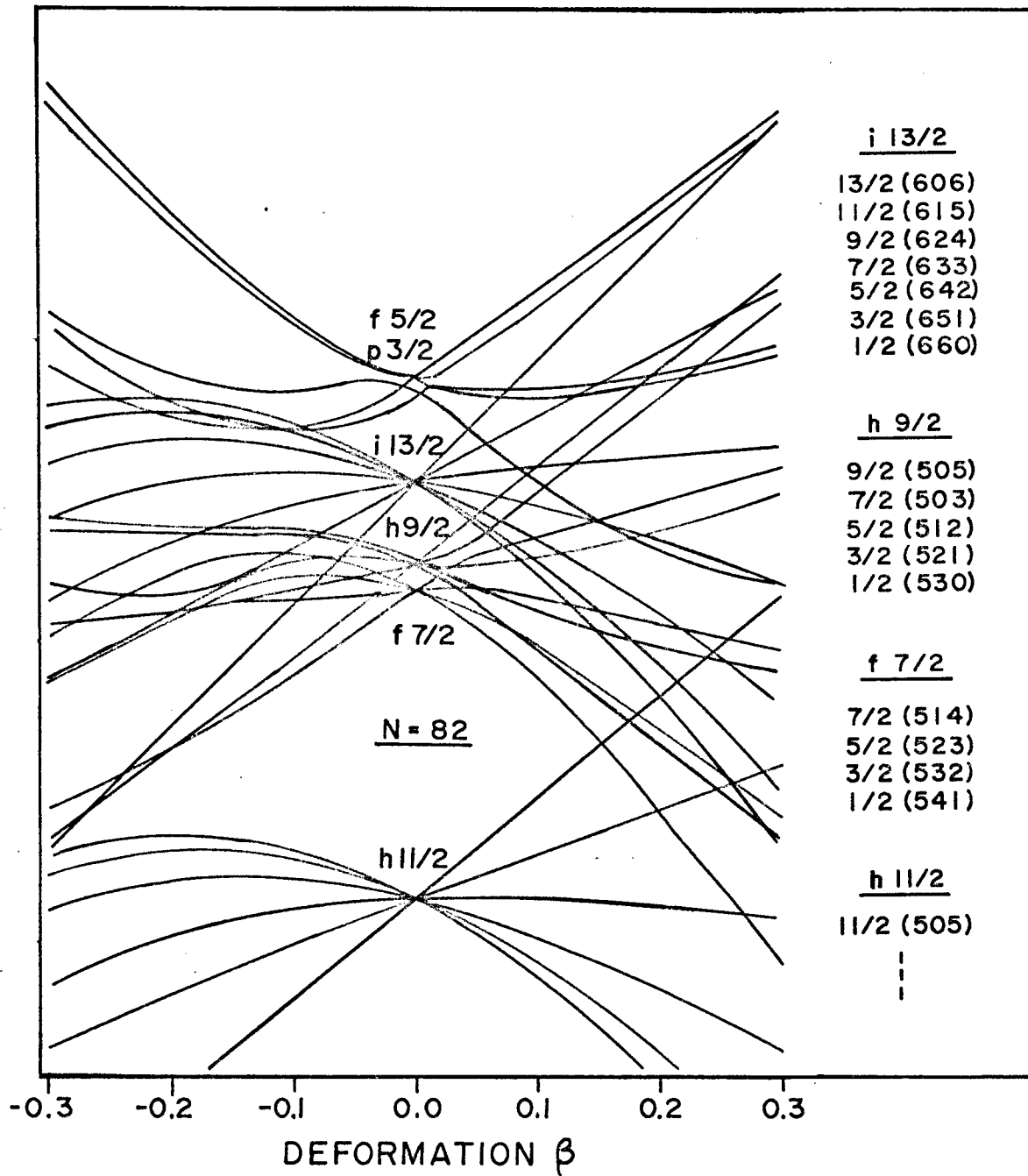


Fig. 2.1 Nilsson diagram for neutron levels in the region $N=90$.

over a wide range of energies. The name "optical" was the result of the similarity of nuclear scattering to the scattering of light by a "cloudy crystal ball". The effect of a nuclear potential on the wavelength of an incident projectile is to change it in the same way that light waves are influenced entering a medium with a different refractive index. By including an imaginary part in the potential, the possibility of absorption is also introduced.

In the optical model, the nucleus is represented by a complex potential which often includes a spin-orbit interaction term. In general, this potential is of the form:

$$U(r) = U_c(r) + V f_v(r) + iW f_w(r) + i W_D f_D'(r) - V_S \left(\frac{1}{r}\right) f_s'(r) \vec{l} \cdot \vec{s}$$

where $f(r)$ may be any suitable potential, but is usually taken to be the Woods-Saxon potential, so that:

$$f_x(r) = \left[1 + \exp \left(\frac{r - r_x A^{1/3}}{a_x} \right) \right]^{-1}$$

and $U_c(r)$ is the Coulomb potential. Thus V , W , W_D , V_S , r_x and a_x are optical-model parameters for the calculation of the nuclear potential. The imaginary terms in the potential take into account the strength of interactions which tend to absorb the projectile, and the terms which involve the derivative of the Woods-Saxon potential tend to concentrate the interaction strength at the surface of the nucleus

rather than to spread it out through the entire volume. By solving the Schrödinger equation in this type of potential the appropriate scattering and reaction cross sections may be obtained.

2.2 Direct Reactions

The distinction between direct and compound-nucleus reactions is essentially dependent on the lifetime of the interaction between the incident projectile and the target nucleus. In a direct reaction process, the projectile passes rapidly through the region of the target potential, interacting with it for only a short period of time (10^{-22} sec). A compound nucleus, however, is formed when the projectile is absorbed and its energy is shared through many collisions, with the eventual decay of the compound nucleus occurring when sufficient energy becomes concentrated on one or more nucleons that they can escape. For this work, only direct reactions with single-step processes will be considered.

2.2.1 Two-nucleon Transfer Reactions*

Several different types of two-nucleon transfer reactions are possible, but for simplicity only the special case of the pick-up reaction (p,t) will be considered in this discussion. The pick-up reaction results from a strong

* A more complete discussion of two-nucleon transfer reactions may be found in Austern (1970) and Glendenning (1965).

interaction between the incident proton, as it passes near the target nucleus, and two outer neutrons. This interaction causes the formation of a triton which is emitted from the potential. Since the (p,t) reaction is a direct reaction process, the angular distribution of the outgoing tritons will tend to be peaked in the forward direction when the energies are above the Coulomb barrier.

For both single and two-nucleon transfer reactions, the angular distributions are characterized by the orbital angular momentum transferred in the reactions.

For the single-nucleon transfer reaction, the transferred angular momentum is carried by one particle and the reaction cross section is roughly proportional to the occupation probability of a nuclear state with that angular momentum. However, in the case of two-nucleon transfer reactions, the orbital angular momentum is carried by a pair of particles, and therefore many different configurations of the two particles may contribute. Thus the form factor is the coherent sum over these shell model configurations. In addition, a coherent sum over different radial states is required to completely describe the centre of mass motion of the transferred pair. For (p,t) reactions, the greatest reaction cross section should be for transitions which proceed by the transfer of a pair of neutrons ($l=0$, spins antiparallel), without the rearrangement of the core nucleons. Since the pairing energy is roughly 1.1 MeV (Meridith et al. 1972), pairing theory predicts

that the ground states of these nuclei will be highly superconducting. This high degree of pair correlation results in a form factor, for the ground state to ground state transition, in which all of the terms add in phase (Yoshida 1962). Thus a strong reaction cross section is expected for this (p,t) transition.

In general, much of the theory for single-neutron transfer reactions applies to two-neutron transfer if one considers the neutron pair as a single particle located at the centre of mass of the pair. The calculation of theoretical results for the two neutron pick-up reaction is discussed in Appendix A1.

CHAPTER III

THE EXPERIMENT

3.1 Experimental Apparatus and Procedure

The two-neutron pick-up reactions $^{149,151,152}\text{Sm}(p,t)$ $^{147,149,150}\text{Sm}$ were performed using 18 MeV protons from the McMaster University F.N. Tandem Van de Graaff accelerator. For the experiment, the proton beam was directed into the target hall housing the Enge split-pole magnetic spectrograph. Focussing of the beam was accomplished by sets of magnetic quadrupole lenses positioned at several points along the beam line.

The experimental arrangement in the target chamber of the magnetic spectrograph is shown in Fig. 3.1. A Si(Li) monitor detector, 1 mm thick with an aperture 0.178" in diameter, was mounted 15 cm from the target at an angle of 45° to the beam direction. In order that the elastically scattered protons would be stopped in the detector, aluminum 0.041" thick was placed in front of the detector. Since the straggling introduced by the aluminum was approximately 300 keV, it was still possible to resolve the elastic-proton peaks due to samarium and carbon, which were separated by about 800 keV. Pulses from the monitor counter were simultaneously recorded by a multichannel analyzer and a single channel analyzer gated on the samarium elastic proton peak. The spectrum from the multichannel analyzer was

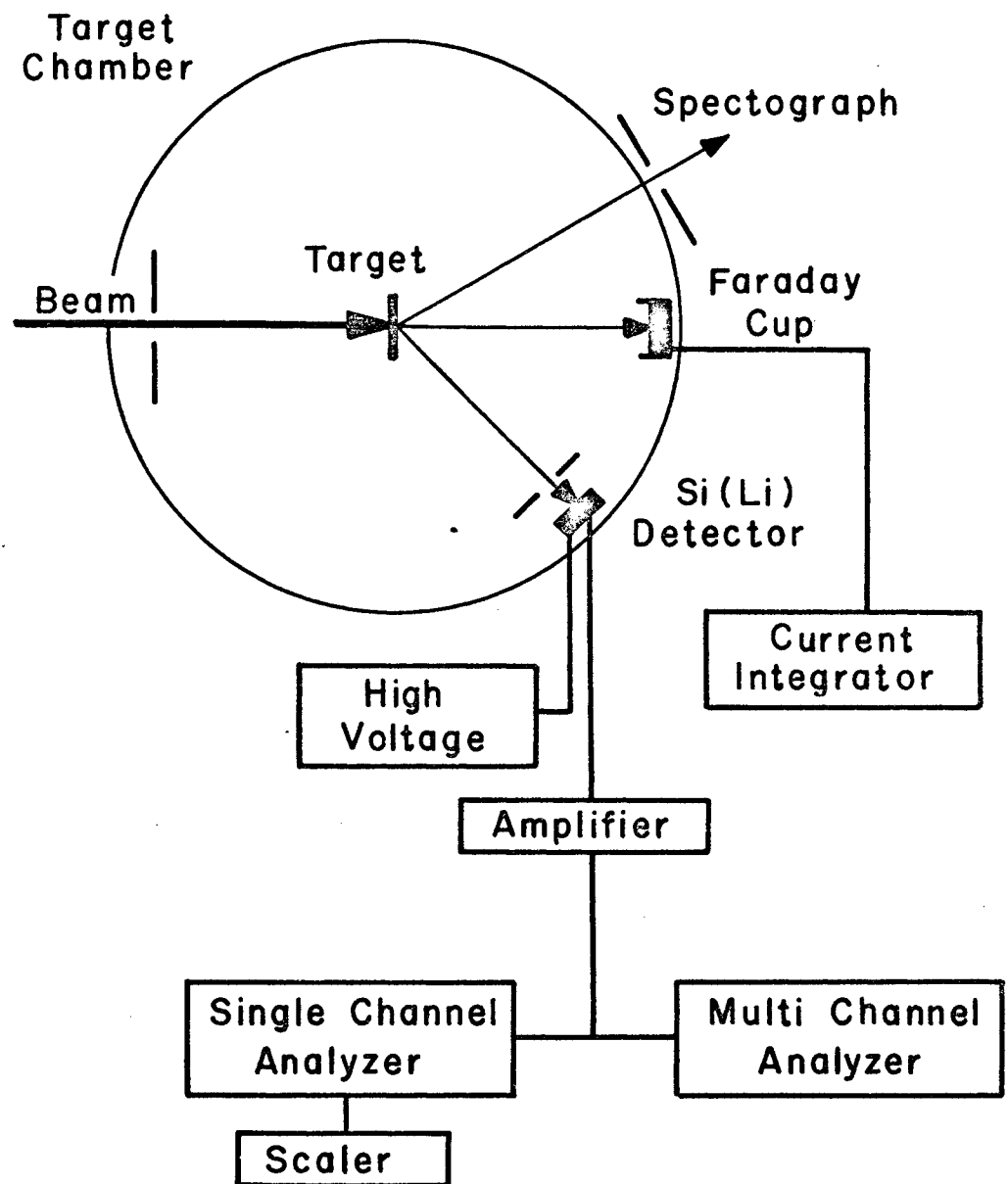


Fig. 3.1 Experimental set-up in the target chamber showing the electronics used.

later used in the determination of absolute cross sections for the (p,t) transitions. To guard against the possibility of the beam hitting the Faraday cup and sputtering brass onto the target, the cup was shielded and lined with tantalum.

To analyze the outgoing tritons from the (p,t) reactions, a split-pole broad-range magnetic spectrograph of the type described by Spencer and Enge (1967) was used. The focussing characteristics of this instrument, for rays of particles of two different momenta which enter the magnet aperture with a small angular spread, are shown in Fig. 3.2. Since the positions of the particle groups on the focal plane depend on the momenta of the reaction products, for reaction products of the same mass (same particles), the plate position of a peak is directly related to the energy of a nuclear level and the intensity of that peak is proportional to the population probability of the level.

Identification of impurities which are significantly different in mass from the major component in the target is also facilitated by the spectrograph. Since the focussing of the reaction products on the focal plane depends on the recoil energy loss and hence the mass of the target nucleus, peaks due to target impurities which are significantly different in mass from the target nucleus appear broadened. These impurity peaks will also seem to move with respect to those due to the target nucleus as the angle of the spectro-

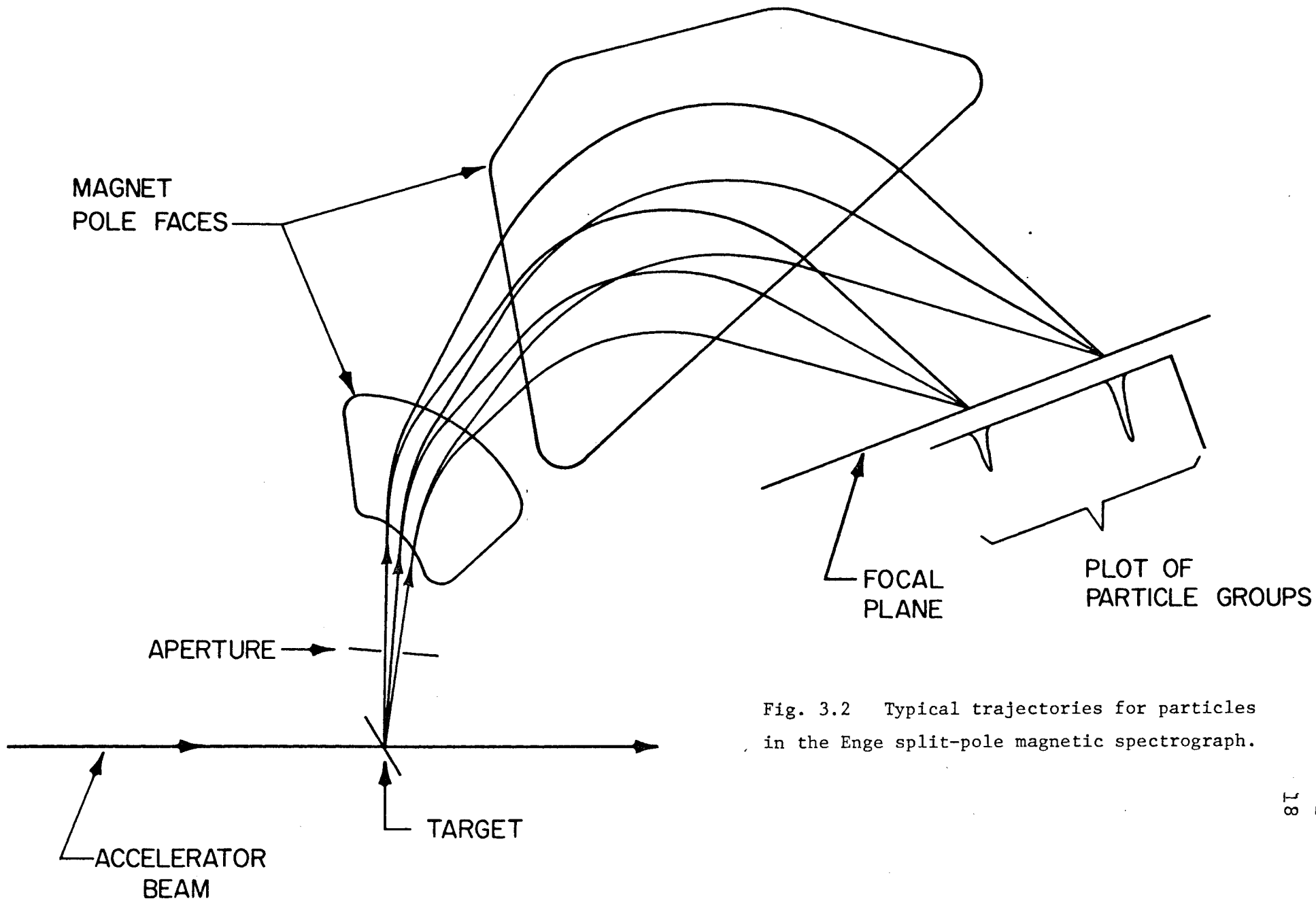


Fig. 3.2 Typical trajectories for particles in the Enge split-pole magnetic spectrograph.

graph is varied. A difference in mass as small as 5 amu will result in an observable change in the positions of impurity peaks with respect to the target peaks over a change in spectrograph angle of about 75° . A search was made for peaks in the observed spectra for this experiment, for all possible impurities within 10 amu of the mass of the target nucleus.

The triton spectra from the (p,t) reactions were recorded on Kodak NTB-50 nuclear emulsions. The photographic plates were mounted in a three-sided rotatable cassette. Since two exposures could be made on one set of emulsions, it was possible to make a maximum of six separate exposures with each loading of the cassette. Aluminum absorbers 0.10 mm thick were placed in front of the plates to stop any recoiling carbon ions from the carbon target backing. For the $^{151}\text{Sm}(p,t)$ reaction, measurements were made at 16 angles between 6° and 80° . The $^{152}\text{Sm}(p,t)$ experiment was performed at laboratory angles of 20° , 25° and 30° just prior to the $^{151}\text{Sm}(p,t)$ studies and using the same experimental set up. Measurements were also made at 6 angles between 15° and 45° for the $^{149}\text{Sm}(p,t)$ experiment which followed the reaction on the ^{151}Sm target.

The target of radioactive ^{151}Sm was prepared from Sm_2O_3 , isotopically enriched in ^{151}Sm , which was purchased from Oak Ridge National Laboratory. The preparation of the target is described in detail in Appendix A2. The

isotopic composition of the target of ^{151}Sm is listed along with those for the other targets used in the experiment in Table 3.1. Impurities of ^{139}La from the reduction of the samarium oxide and of ^{151}Eu which is the daughter product of the ^{151}Sm beta decay were also found to be present in the $^{151}\text{Sm}(p,t)$ spectra.

3.2 Results and Discussion

Two typical triton spectra from the $^{151}\text{Sm}(p,t)$ reaction are shown in Fig. 3.3. The peak widths (FWHM) are approximately 10 keV. The first spectrum, at a laboratory angle of $\theta=15^\circ$, was found to be near a minimum in the $\ell=0$ angular distribution and the second spectrum, at $\theta=25^\circ$, corresponded to a maximum. Because of the low background in this experiment, it was possible to obtain angular distributions for peaks which were as small as 2% of the most intense peak in the spectrum and this analysis yielded the large number of $\ell=0$ transfer peaks indicated in Fig. 3.3.

The absolute cross sections for the peaks which correspond to levels in ^{149}Sm have been listed in Table 3.2. To convert from the number of tracks observed in a peak to the absolute cross section for that peak, a normalization procedure described by the following formula was used:

$$\left(\frac{d\sigma}{d\Omega}\right)_{\text{spectrograph}} = \left(\frac{d\sigma}{d\Omega}\right)_{\text{monitor elastic}} \cdot \frac{d\Omega_{\text{monitor}}}{d\Omega_{\text{spectrograph}}} \cdot \frac{100\%}{\text{isotopic \%}}$$

$$\cdot \frac{N_{\text{spectrograph}}}{N_{\text{monitor}}}$$

Table 3.1

Isotopic compositions (%) and approximate thicknesses* of the targets

Target	^{144}Sm	^{147}Sm	^{148}Sm	^{149}Sm	^{150}Sm	^{151}Sm	^{152}Sm	^{154}Sm	Thickness ($\mu\text{g}/\text{cm}^2$)
^{149}Sm	<0.08	0.33	0.55	97.46	0.65	—	0.70	0.30	~30
^{151}Sm	—	0.89	0.04	0.16	2.95	88.86	6.84	0.25	~60
^{152}Sm	<0.01	0.08	0.07	0.12	0.10	—	99.18	0.45	~25

* Target thicknesses were determined from elastic scattering of 18 MeV protons.

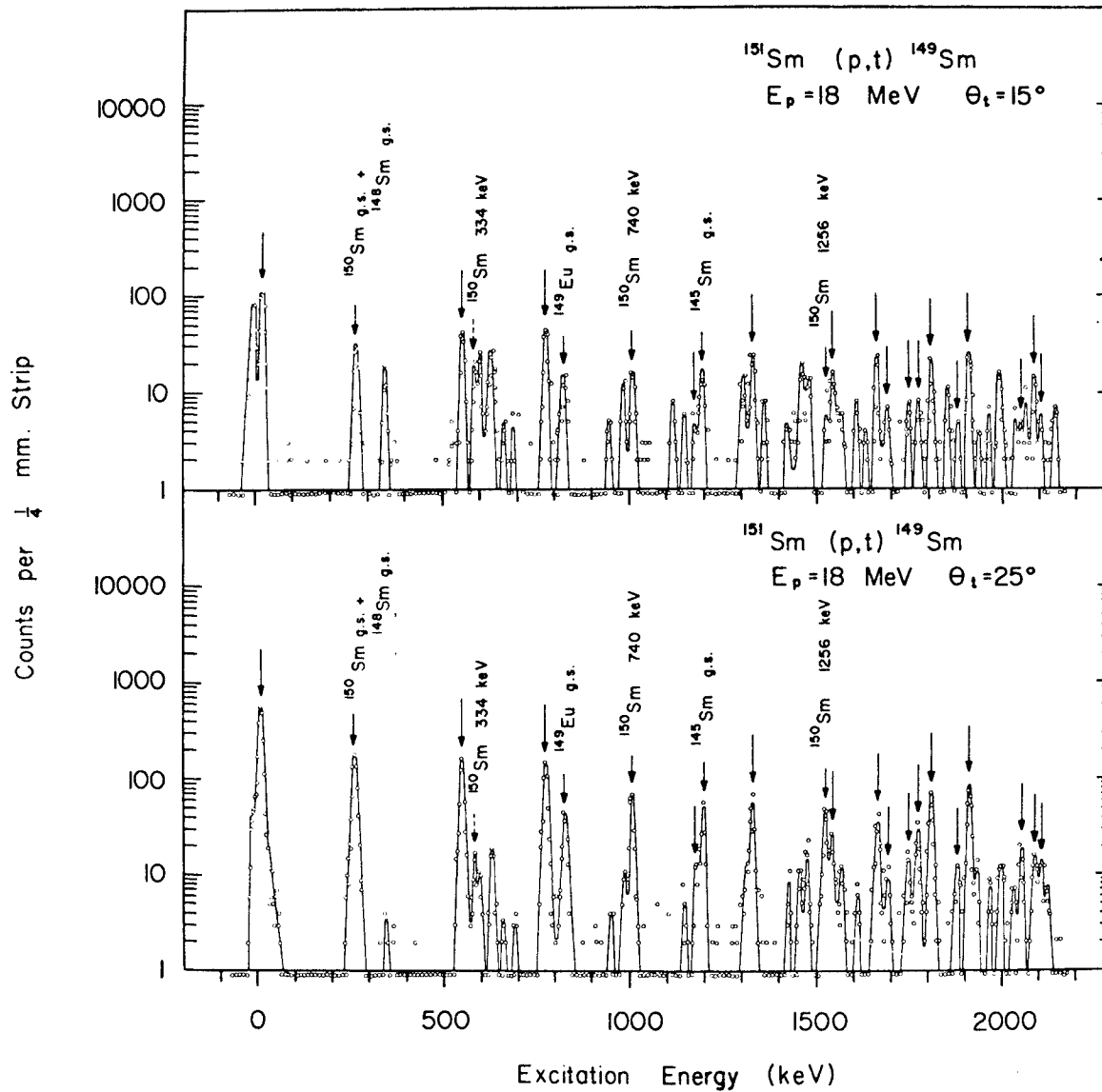


Fig. 3.3 Triton spectra from the $^{151}\text{Sm}(p,t)^{149}\text{Sm}$ reaction. The solid arrows indicate peaks which have a typical $\ell=0$ angular distribution. Impurity peaks are labelled by the level in the final nucleus.

Table 3.2

Cross sections for (p,t) transitions to levels in ^{149}Sm

Energy (keV)	Cross section ($\mu\text{b}/\text{sr}$)		
	$\theta=15^\circ$	$\theta=25^\circ$	ℓ transfer
0	41	17	2 (?)
22.5	45	262	0
~ 286	<5	<25	0 (?)
352	6	3	
560	18	68	0
606	9	4	
638	16	8	
785	19	75	0
997	4	4	
1124	4	2	
1187	2	8	0
~ 1207	<4	<18	0 (?)
1325	7	8	
1339	11	26	0
1472	9	5	
1487	4	8	
1548	8	10	0
1558	2	4	
1581	3	5	
1674	8	20	0
1699	4	5	0
1759	4	7	0
1782	5	13	0
1817	7	35	0
1891	2	6	0
1919	11	35	0
1993	2	4	
2005	5	4	
2061	2	7	0
2099	5	10	0
2116	3	5	0

The value of $\left(\frac{d\sigma}{d\Omega}\right)_{\text{monitor elastic}}$, the elastic proton cross section at $\theta=45^\circ$, was taken to be 352 mb/sr as calculated by the DWBA program. The ratio of the solid angles for the monitor counter and the spectragraph was determined from the geometric dimensions of the apertures used. The data from the samarium peak in the monitor spectrum were used to calculate the number of events in the monitor, N_{monitor} . To correct for isotopic impurities in the target, the percentage of the target which was composed of the isotope of interest, isotopic %, was used. The accuracy of absolute cross sections determined by this procedure should be better than 20% for strong peaks and somewhat poorer for weak peaks. However, the relative cross sections for a particular state at different angles should be accurate to better than 10%. The probable errors in the excitation energies listed in Table 3.2 are roughly 3 keV.

The 22.5 keV state in ^{149}Sm , which has been previously assigned as $I^\pi=5/2^-$ (Lederer et al. 1967), is shown in Table 3.2 to have a cross section similar to that of the ground state at $\theta=15^\circ$, but at $\theta=25^\circ$, where the $\ell=0$ transfer has a maximum in its angular distribution, the cross section of the 22.5 keV level has increased by almost a factor of 6. This $\ell=0$ transfer from the ground state of ^{151}Sm to the 22.5 keV level in ^{149}Sm lends strength to the negative parity assignment by Nelson et al. (1971) of the spin 5/2 ground state of ^{151}Sm (Robertson et al. 1971). The 286 keV peak, which is

also expected to have $I^\pi=5/2^-$ (Lederer et al. 1967), was not resolved from peaks due to isotopic impurities of ^{152}Sm and ^{150}Sm in the target. A peak due to an isotopic impurity of ^{147}Sm also obscured the 1207 keV level in ^{149}Sm . As a result, there is uncertainty in the energies of these levels, and the cross sections quoted in Table 3.2 are only upper limits.

The assignments of $\ell=0$ transitions to levels in ^{149}Sm , as indicated in the final column of Table 3.2, were based on the characteristic angular distributions shown in Fig. 3.4. The curves drawn through the experimental points result from DWBA calculations using the program DWUCK, assuming a spherical form factor for all transitions. The calculation was performed using the optical model parameter set DX of Fleming et al. (1970) and assuming that a pair of neutrons was removed from the $1h_{9/2}$ shell by the reaction. It was empirically determined (Appendix A1) that the shape of the DWBA curve was relatively insensitive to the choice of potential and the choice of the neutron shell. The neutron binding energy was adjusted to yield the two neutron separation energy of Meredith et al. (1972). Increasing the excitation energy resulted in variations in the depths and positions of some of the minima in the calculated angular distributions as shown in Fig. 3.4.

The angular distributions for several other levels in ^{149}Sm did not display the characteristic shapes of $\ell=0$ transitions and these are shown in Fig. 3.5. In this case the

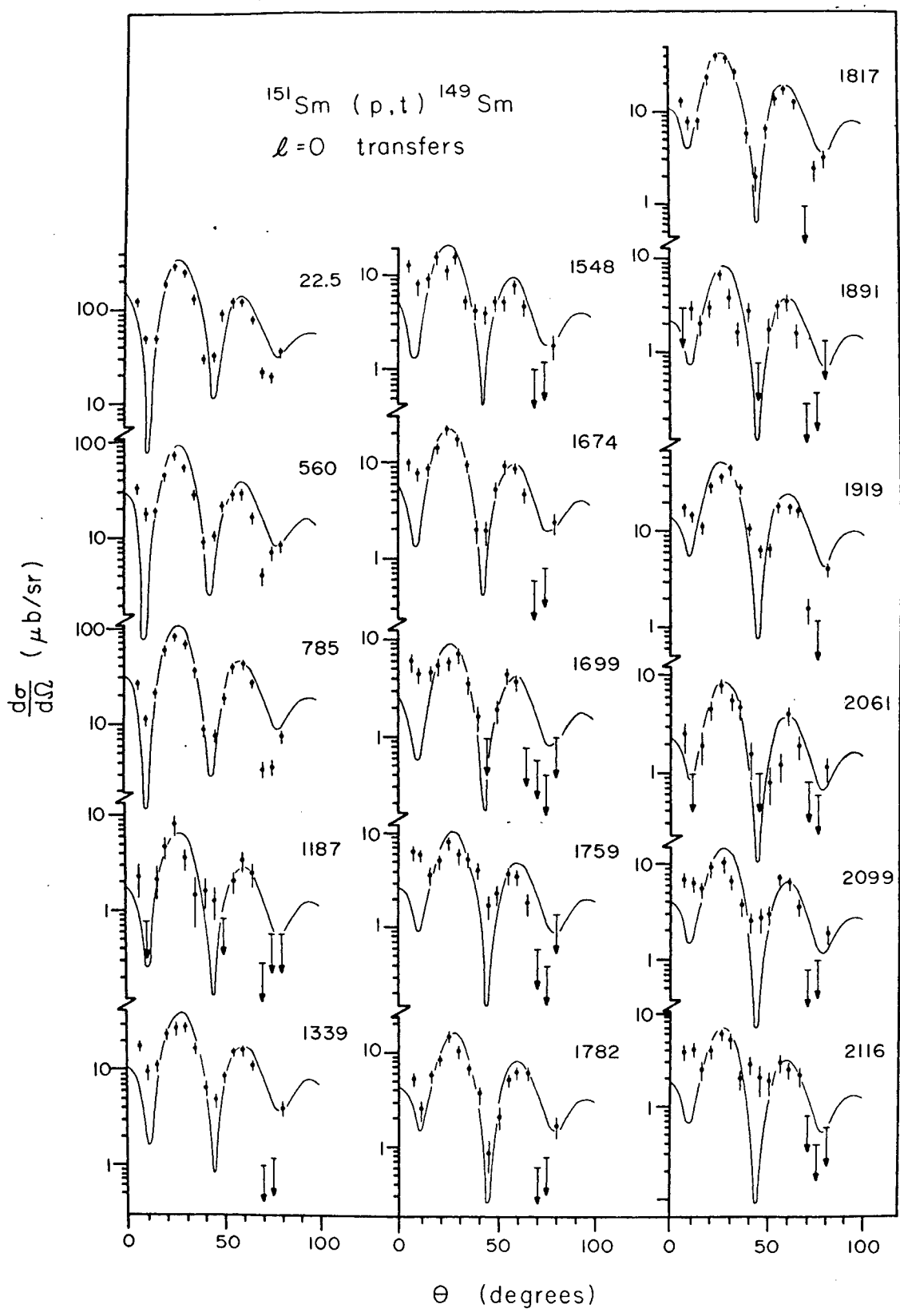


Fig. 3.4 Angular distributions for $\ell=0$ transitions to levels in ^{149}Sm . Arrows indicate upper limits on the cross section.

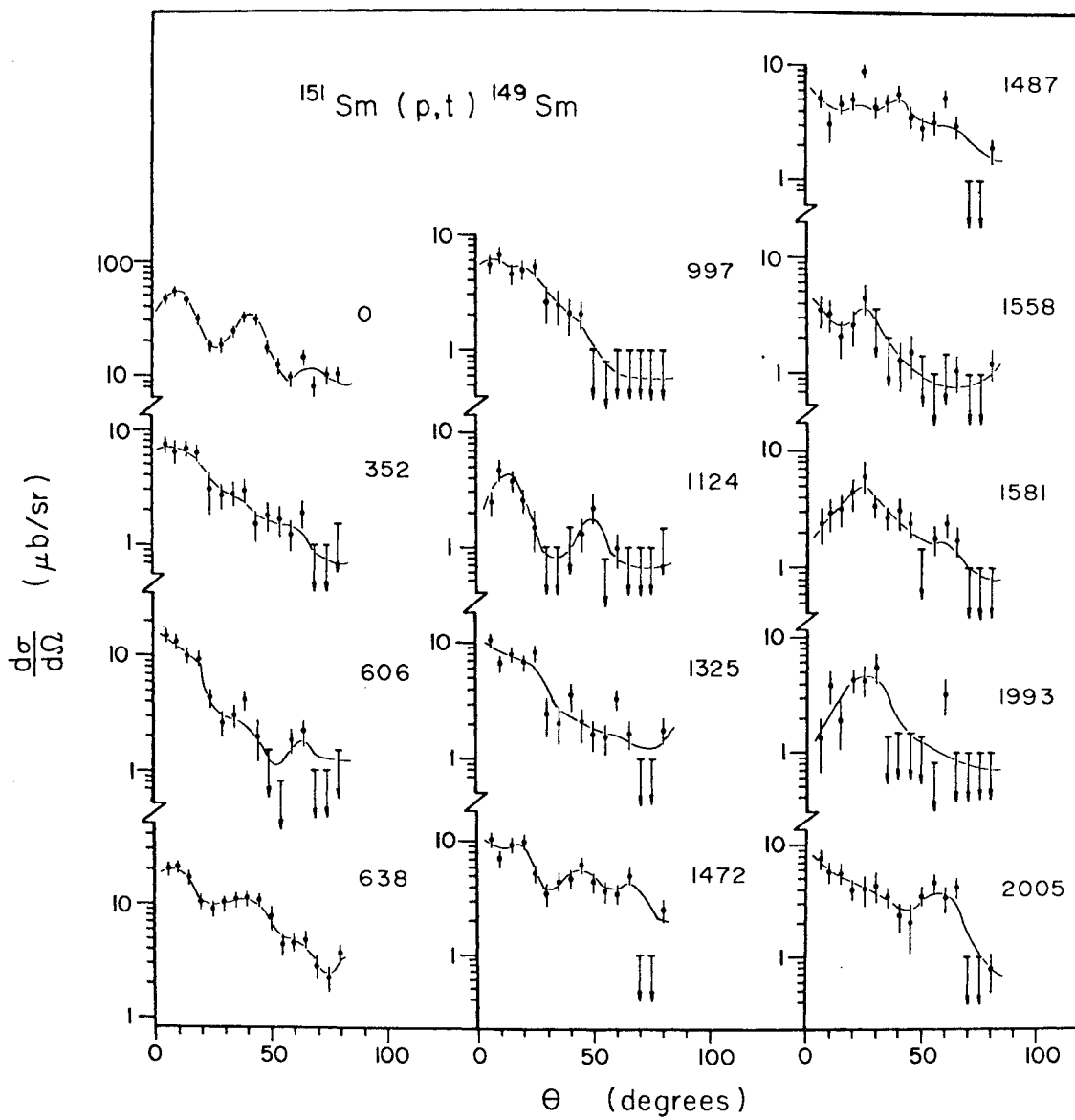


Fig. 3.5 Angular distributions for transitions to other levels in ^{149}Sm . Arrows indicate upper limits on the cross section.

curves drawn through the experimental points are merely to guide the eye and do not represent theoretical curves. In fact, with the exception of the ground state angular distribution which was similar to that of a $1h_{9/2} \ell=2$ transition, the experimental angular distributions of Fig. 3.5 were not well reproduced by either $\ell=2$ or $\ell=4$ DWBA calculations, done in the same manner as the $\ell=0$ calculations, assuming the removal of a neutron pair from either the $1h_{9/2}$ or $2f_{7/2}$ shell. The results of the DWBA calculations are shown in Fig. A1.3. A similar variation in the shape of measured angular distributions for $\ell=2$ transitions has been observed in the even isotopes of samarium by McLatchie et al. (1970) and in the even isotopes of gadolinium by Elze et al. (1972).

Since the total $\ell=0$ cross section for (p,t) reactions on even samarium targets varies only slowly with changes in mass (McLatchie et al. 1970) a comparison of the total $\ell=0$ cross section observed in the $^{151}\text{Sm}(p,t)$ reaction to the total $\ell=0$ cross section for the $^{152}\text{Sm}(p,t)$ reaction has been made in Fig. 3.6. The cross sections for the relevant levels in the $^{152}\text{Sm}(p,t)$ reaction are listed in Table 3.3. With the exception of the ground state, only levels populated by $\ell=0$ transfers are shown in Fig. 3.6. The sum of the $\ell=0$ strengths observed in the $^{151}\text{Sm}(p,t)$ reaction below 2.2 MeV excitation in ^{149}Sm amounts to less than 75% of that observed in the $^{152}\text{Sm}(p,t)$ reaction. This reduction in the observed $\ell=0$ strength cannot be attributed to the Q-value dependence

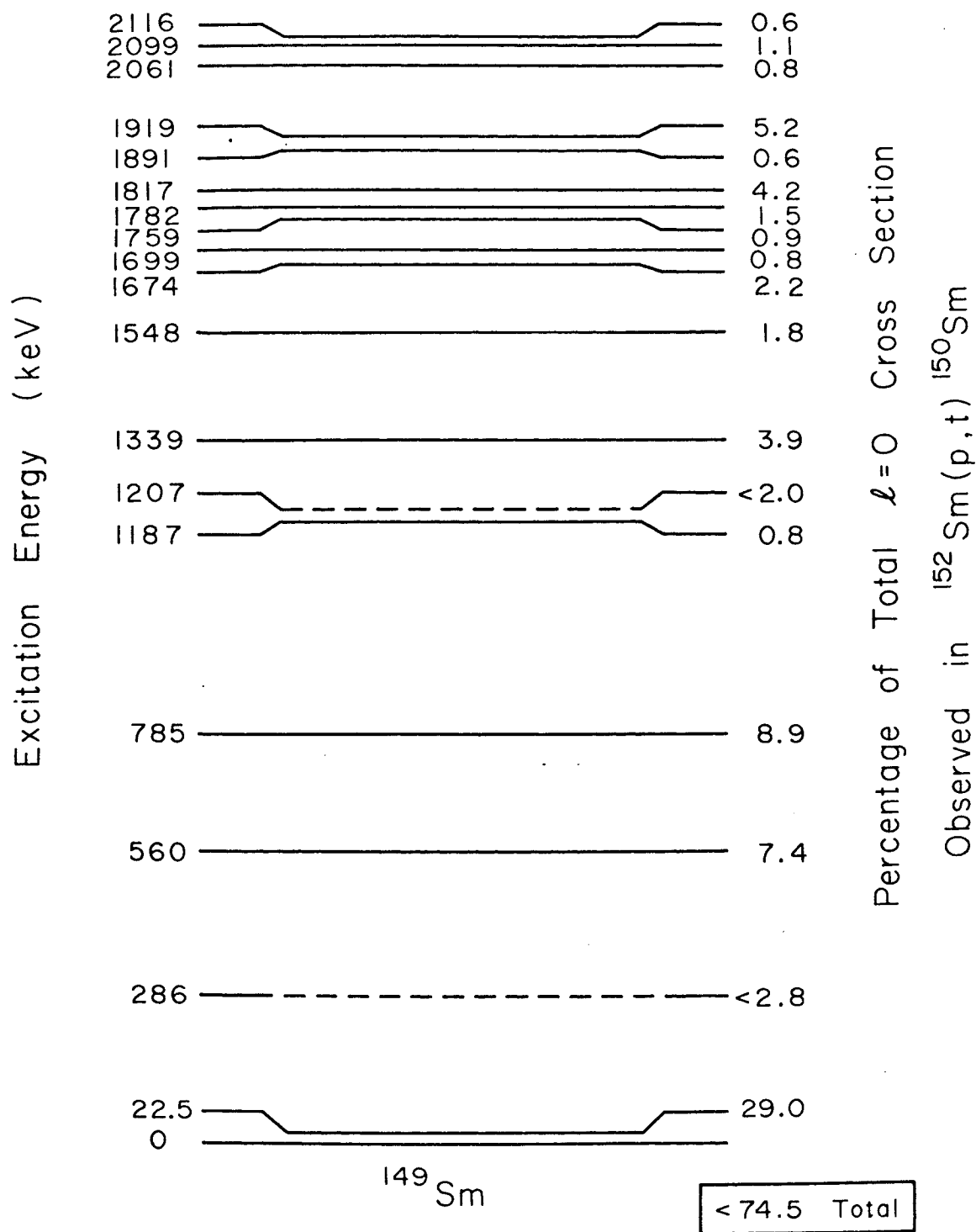


Fig. 3.6 Intensities of $\ell=0$ transitions in the $^{151}\text{Sm}(p,t)$ reaction expressed as percentages of the total $\ell=0$ cross section observed in the $^{152}\text{Sm}(p,t)^{150}\text{Sm}$ reaction. The levels shown dashed are ones for which the energies and cross sections are uncertain due to isotopic impurities.

Table 3.3

Absolute cross sections for selected levels* in ^{150}Sm

Energy (keV)	Cross section ($\mu\text{b}/\text{sr}$)		
	$\theta=20^\circ$	$\theta=25^\circ$	$\theta=30^\circ$
0	264	386	371
740	187	264	279
1256	112	178	213

* Levels listed are the strong components of $\ell=0$ cross section in the $^{152}\text{Sm}(p,t)$ reaction.

of the reaction cross section.

In the case of the $^{149}\text{Sm}(p,t)^{147}\text{Sm}$ reaction, where both nuclei are "spherical", only one strong $\ell=0$ transition was found. Fig. 3.7 shows a typical triton spectrum from this reaction. All of weak peaks shown, which may correspond to excited states in ^{147}Sm , were less than 2% of the intensity of the ground state transition. The angular distribution of the ground state is shown in Fig. 3.8 and the curve drawn through the experimental points is the $\ell=0$ DWBA calculation for the removal of a pair of neutrons from the $2f_{7/2}$ shell. With cross sections at $\theta=15^\circ$ and $\theta=25^\circ$ of $176\mu\text{b}/\text{sr}$ and $632\mu\text{b}/\text{sr}$ respectively, the ground state to ground state transition in the $^{149}\text{Sm}(p,t)$ reaction accounted for about 85% of the total $\ell=0$ cross section observed in the $^{152}\text{Sm}(p,t)$ experiment.

The isotopic impurity of ^{152}Sm in the target of ^{151}Sm made it possible to obtain a more complete angular distribution for the $\ell=0$ transitions to levels in ^{150}Sm than had been anticipated prior to the experiment. Fig. 3.9 shows the angular distributions for these levels. The curves drawn through the experimental points are the result of DWBA calculations for $\ell=0$ transitions in the $^{152}\text{Sm}(p,t)$ reaction where a pair of neutrons are removed from the $1h_{9/2}$ shell. The absolute cross sections obtained for the ^{152}Sm impurity have been normalized to those listed in Table 3.3 for the (p,t) reaction on the ^{152}Sm target.

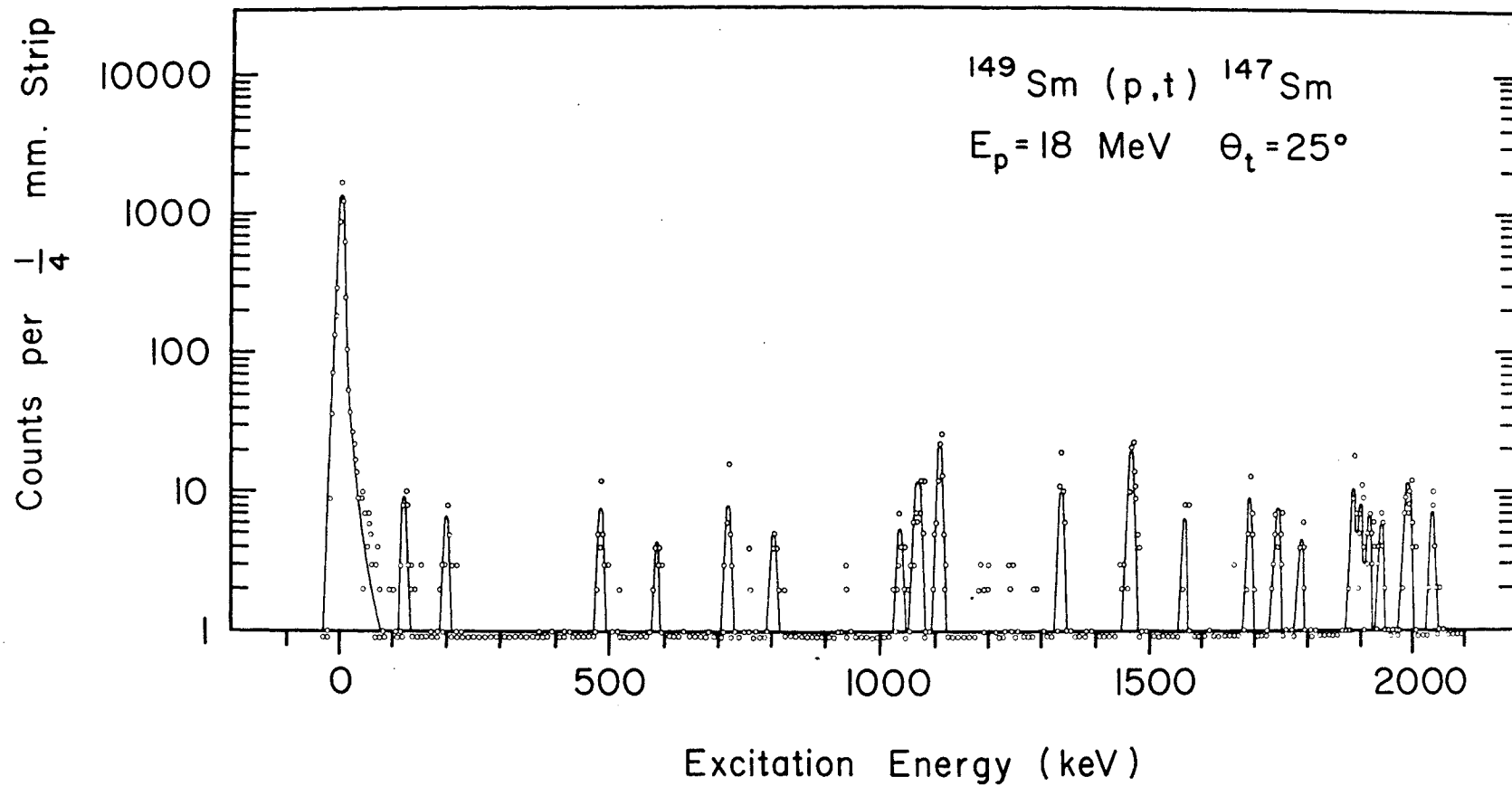


Fig. 3.7 Triton spectrum from the $^{149}\text{Sm}(p,t)^{147}\text{Sm}$ reaction.

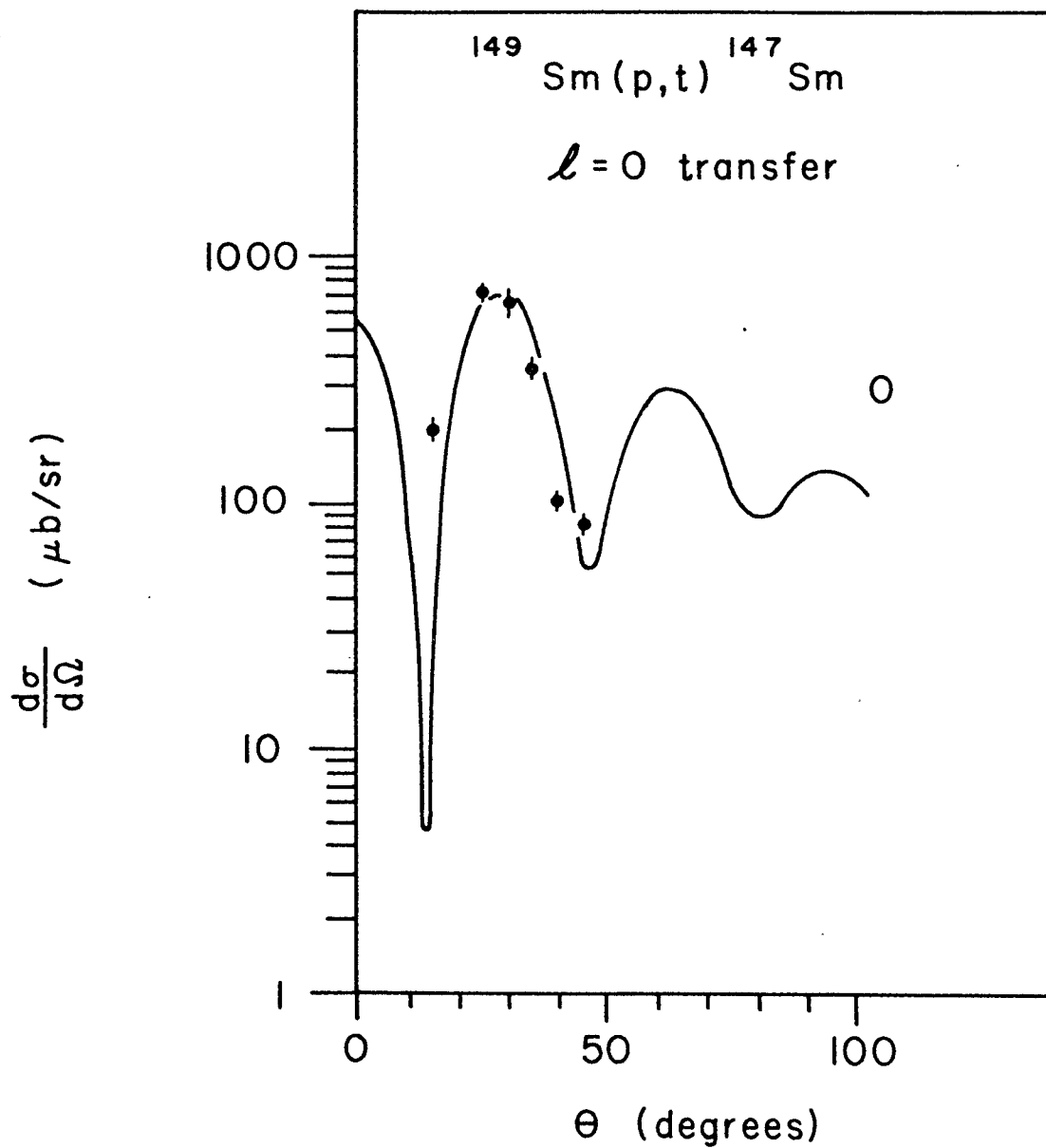


Fig. 3.8 The angular distribution of the ground state of ^{147}Sm populated by the $^{149}\text{Sm}(p,t)$ reaction.

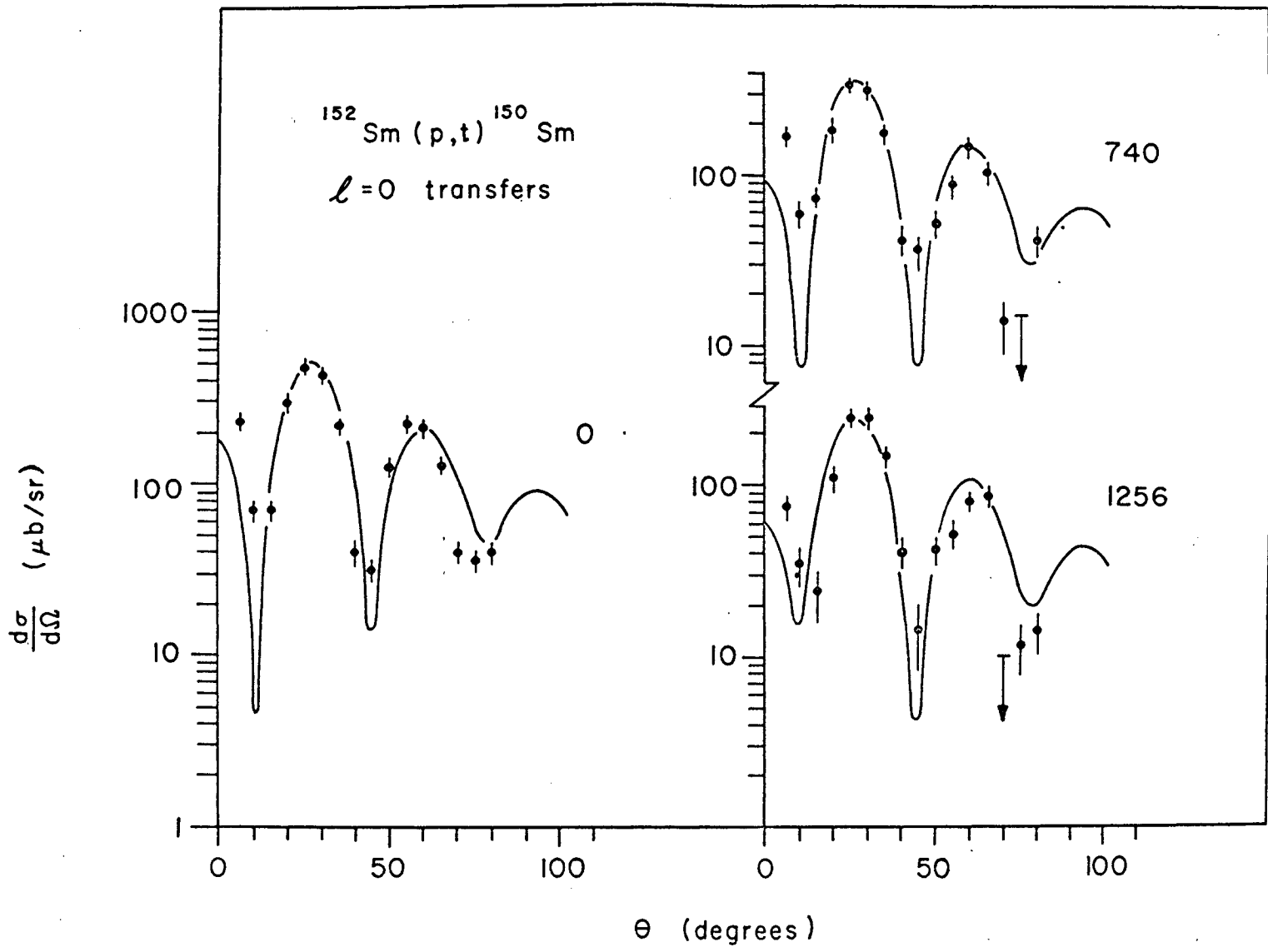


Fig. 3.9 Angular distributions for $l=0$ transitions to levels in ^{150}Sm as determined from the ^{152}Sm impurity in the ^{151}Sm target. Only the 740 keV level can be attributed solely to the ^{152}Sm impurity.

During the course of the $^{152,151,149}\text{Sm}(p,t)$ experiments short calibration exposures were made using elastically scattered protons in order to obtain precise values of the beam energy for Q-value calculations. The reaction Q-values, listed in Table 3.4, were found to yield two neutron separation energies which were in excellent agreement with those tabulated by Meredith et al. (1972).

3.3 Summary

In the $^{152}\text{Sm}(p,t)$ reaction about 45% of the total $\ell=0$ strength appeared in the ground state to ground state transition. This fragmentation of $\ell=0$ strength occurred to an even greater extent in the $^{151}\text{Sm}(p,t)$ reaction. Eighteen $\ell=0$ transitions to excited states were observed and the transition to the 22.5 keV level accounted for approximately 40% of the total $\ell=0$ strength observed in the $^{151}\text{Sm}(p,t)$ reaction. However, for the $^{149}\text{Sm}(p,t)$ reaction, where both the initial and final nuclei are "spherical", only one strong $\ell=0$ transition, to the ground state of ^{147}Sm , was observed. Fig. 3.10 shows the results of the (p,t) experiments on targets of ^{151}Sm and ^{149}Sm along with some preliminary results of recent work by Burke et al. (1972) for the $^{149}\text{Sm}(t,p)$ reaction. These results suggest that, as in the case of two-neutron transfer reactions on even-even target nuclei, the fragmentation of $\ell=0$ strength in (t,p) and (p,t) reactions results from a significant change in the nuclear deformation between the initial and final nuclei.

Table 3.4

Q-values and two-neutron separation energies

Target	Expt. Q-value (keV)	Two-neutron separation energy (keV)	
		Experiment	Mass Tables*
^{149}Sm	$-5,532 \pm 7$	$14,014 \pm 7$	$14,014.6 \pm 1.7$
^{151}Sm	$-5,100 \pm 4$	$13,582 \pm 4$	$13,582.5 \pm 2.3$
^{152}Sm	$-5,376 \pm 4$	$13,858 \pm 4$	$13,857.3 \pm 2.2$

* Meredith et al. (1972)

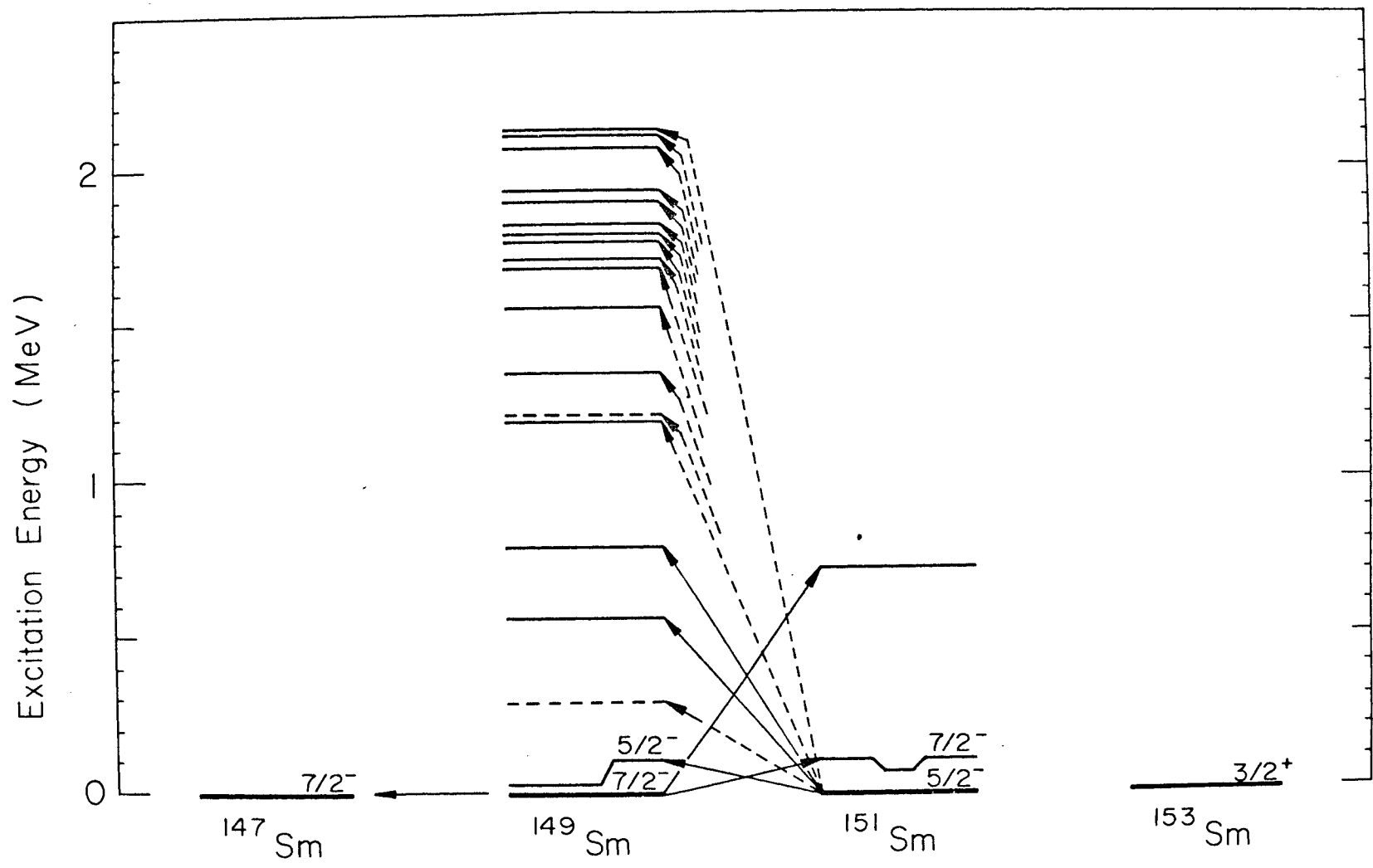


Fig. 3.10 The $\ell=0$ (t,p) and (p,t) transitions in the odd samarium isotopes. Broken arrows indicate $\ell=0$ transitions where the strength is less than 25% of the lowest energy $\ell=0$ transition. Since $\ell=0$ transitions join states of the same spin and parity, $5/2^-$ assignments may be made for all the excited states shown in ^{149}Sm .

Currently two pictures have been suggested for understanding the fragmentation of $\ell=0$ strength in the transition region. For simplicity consider a (p,t) reaction connecting a "deformed" and "spherical" nucleus; the arguments apply equally well for a (t,p) reaction. One of the pictures considers an expansion of the initial "deformed" nucleus in a complete set of orthogonal "spherical" basis states. Naturally such an expansion would require many "spherical" states, each having an overlap with a different state in the final nucleus, to represent a "deformed" ground state. Thus, several $\ell=0$ transfers would be seen. The second picture invokes the idea of partially "spherical" and partially "deformed" states in a nucleus in the transition region. In this way, the amount of overlap between initial and final states would depend on the fraction of spherical or deformed wavefunctions in the initial and final states. Both of these pictures are equivalent representations of the experimental results.

The reduction in the total $\ell=0$ cross section observed in the $^{149,151}\text{Sm}(p,t)$ reactions compared to that of the $^{152}\text{Sm}(p,t)$ reaction may be due in part to "blocking" of one of the possible reaction channels by the odd neutron. This arises from the fact that for isotopes with an odd number of neutrons one of the neutron valence levels is occupied by a single neutron, while for isotopes with an even number

of neutrons all of the neutron valence levels are occupied by neutron pairs. In this way $\ell=0$ transfers, which require neutron pairs, will be "blocked" at that one level. It is possible that a shape hindrance of the (p,t) reaction process occurs in the region of changing nuclear deformation; however, the accuracy of the experimental results is not sufficient to be certain of this difference. The report by McLatchie et al. (1970) indicated that the total $\ell=0$ cross section for the $^{152}\text{Sm}(p,t)$ reaction was about 10% less than that for the $^{154}\text{Sm}(p,t)$ reaction. A similar variation has been found in this work where the total $\ell=0$ cross section for the $^{151}\text{Sm}(p,t)$ reaction was about 10% less than that for the $^{149}\text{Sm}(p,t)$ reaction. It is impossible to say without more accurate experiments whether this apparent reduction in the total $\ell=0$ cross section is significant.

APPENDICES

Appendix A1:DWBA Calculations

The DWBA calculations were done without the inclusion of any reaction channel coupling and assuming a spherical form-factor for all transitions. The calculations were performed using the program DWUCK. Several different optical-model parameter sets (Table A1.1) were tried in the calculations, but only minor changes in the shapes of the $\ell=0$ angular distributions were observed, as shown in the first column of Fig. A1.1. All of the curves displayed in the first column were calculated assuming that a pair of neutrons was being removed from the $2f_{7/2}$ shell by a (p,t) reaction on a target of ^{151}Sm . The optical-model parameter set DX of Fleming et al. (1970) was chosen as the set to be used throughout all further DWBA calculations. The second column of Fig. A1.1 shows the results of $\ell=0$ DWBA calculations assuming the removal of a pair of neutrons from various neutron shells near $N=89$. Since little variation in the shapes of the $\ell=0$ angular distributions was observed, it was decided from theoretical considerations to use the $1h_{9/2}$ neutron shell for (p,t) reactions on targets of ^{151}Sm and ^{152}Sm , and to use the $2f_{7/2}$ neutron shell for $^{149}\text{Sm}(p,t)$ reactions.

As previously indicated in Fig. 2.1, the Nilsson model predicts that for "spherical" nuclei in the region $N\approx 90$, neutron pairs will be found in the $2f_{7/2}$ shell; however, for "deformed" nuclei, levels from the $1h_{9/2}$ and $1i_{13/2}$ shell-model states

Table A1.1
Optical-model parameter sets for DWBA calculations

Channel	Set	V (MeV)	r_V (F)	a_V (F)	W (MeV)	r_W (F)	a_W (F)	W_D (MeV)	r_D (F)	a_D (F)	V_S (MeV)	r_S (F)	a_S (F)	r_C (F)
Proton	A*	46.0	1.33	0.50	9.0	1.33	0.50							1.33
	B*	50.8	1.25	0.65				55.6	1.25	0.47	34.0	1.25	0.65	1.25
	D*	55.7	1.20	0.70				45.2	1.25	0.70	12.0	1.10	0.70	1.20
	R†	57.5	1.17	0.75				40.0	1.32	0.64				1.25
Triton	S†	166.7	1.16	0.75	14.7	1.50	0.82							1.40
	X*	176.0	1.14	0.72	18.0	1.61	0.82							1.14
Bound State	a		1.25	0.65										

* Fleming et al. (1970).

† Maher et al. (1972).

^a Adjusted to give two-neutron separation energies of Meredith et al. (1972).

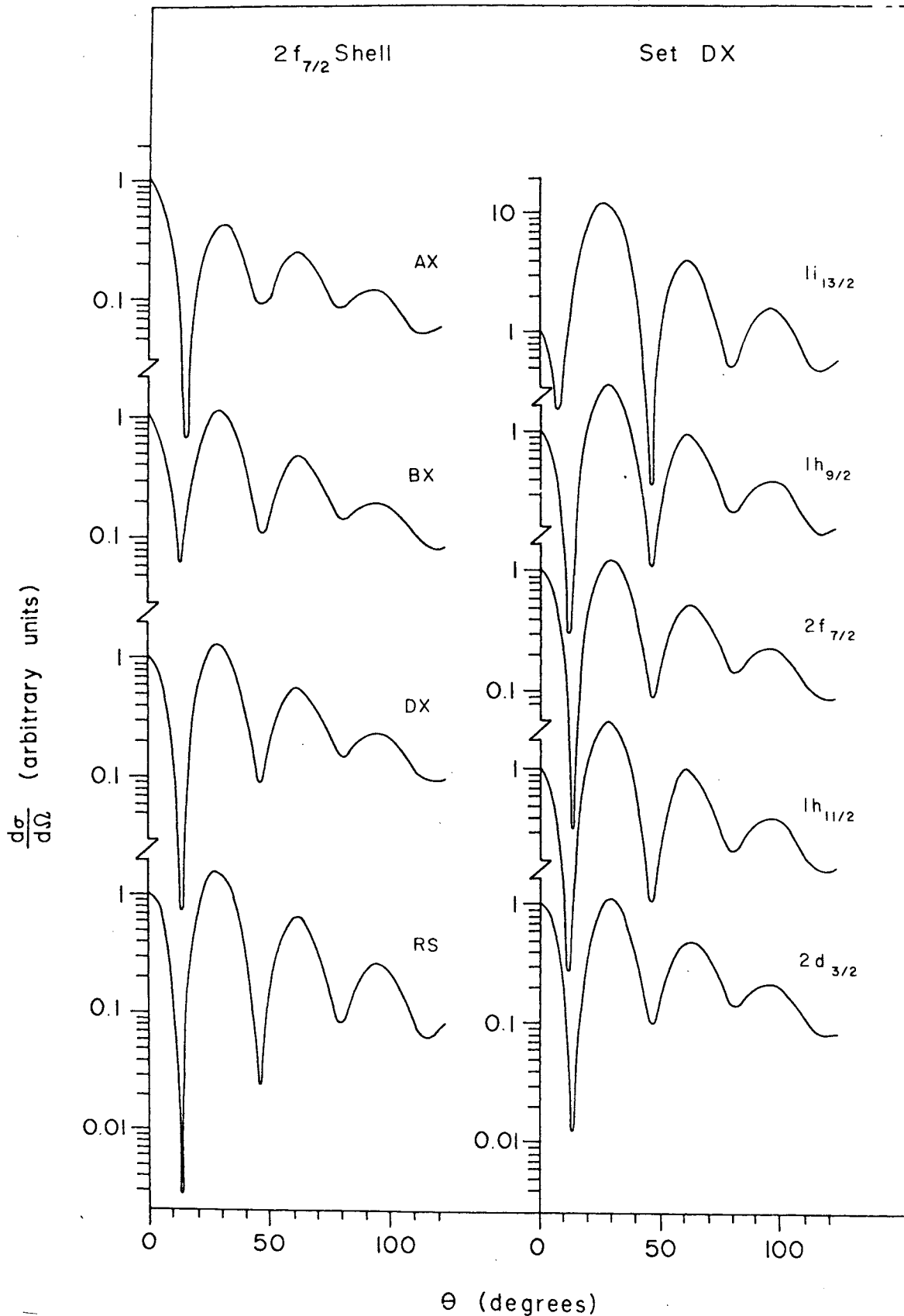


Fig. A1.1 The DWBA angular distributions for $l=0$ transitions in the $^{151}\text{Sm}(p,t)$ reaction using (in the 1st column) several different optical-model potentials and (in the 2nd column) different neutron shells.

become energetically favoured for population by pairs of neutrons. For this reason, DWBA calculations for (p,t) reactions on samarium targets with $N \geq 89$ were performed assuming the removal of a neutron pair from the $1h_{9/2}$ shell and calculations for $N \leq 88$, assuming a $2f_{7/2}$ neutron pair was removed.

Fig. A1.2 shows the effect of varying the proton beam energy on the shape of $\ell=0$ transition angular distribution. The DWBA calculations which generated the curves shown in this figure considered the removal a $1h_{9/2}$ neutron pair in the $^{151}\text{Sm}(p,t)$ reaction at several different beam energies. Notice that the greatest intensity variations in the $\ell=0$ DWBA angular distributions for this reaction occur at 18 MeV, the energy at which the experiment was performed. The increase in the forward peaking of the angular distributions with higher beam energies is characteristic of direct-reaction processes.

The variation in the shape of the $\ell=0$ angular distribution with increasing excitation energy can be seen in Fig. 3.4 or Fig. 3.9 and is not reproduced here. It is interesting to note however, that only minor changes occurred in the depths and positions of some of the minima and only a small variation of less than 25% in 2 MeV, in the reaction cross section as a result of the Q-value dependence was predicted.

Since (p,t) reactions on the even isotopes of samarium

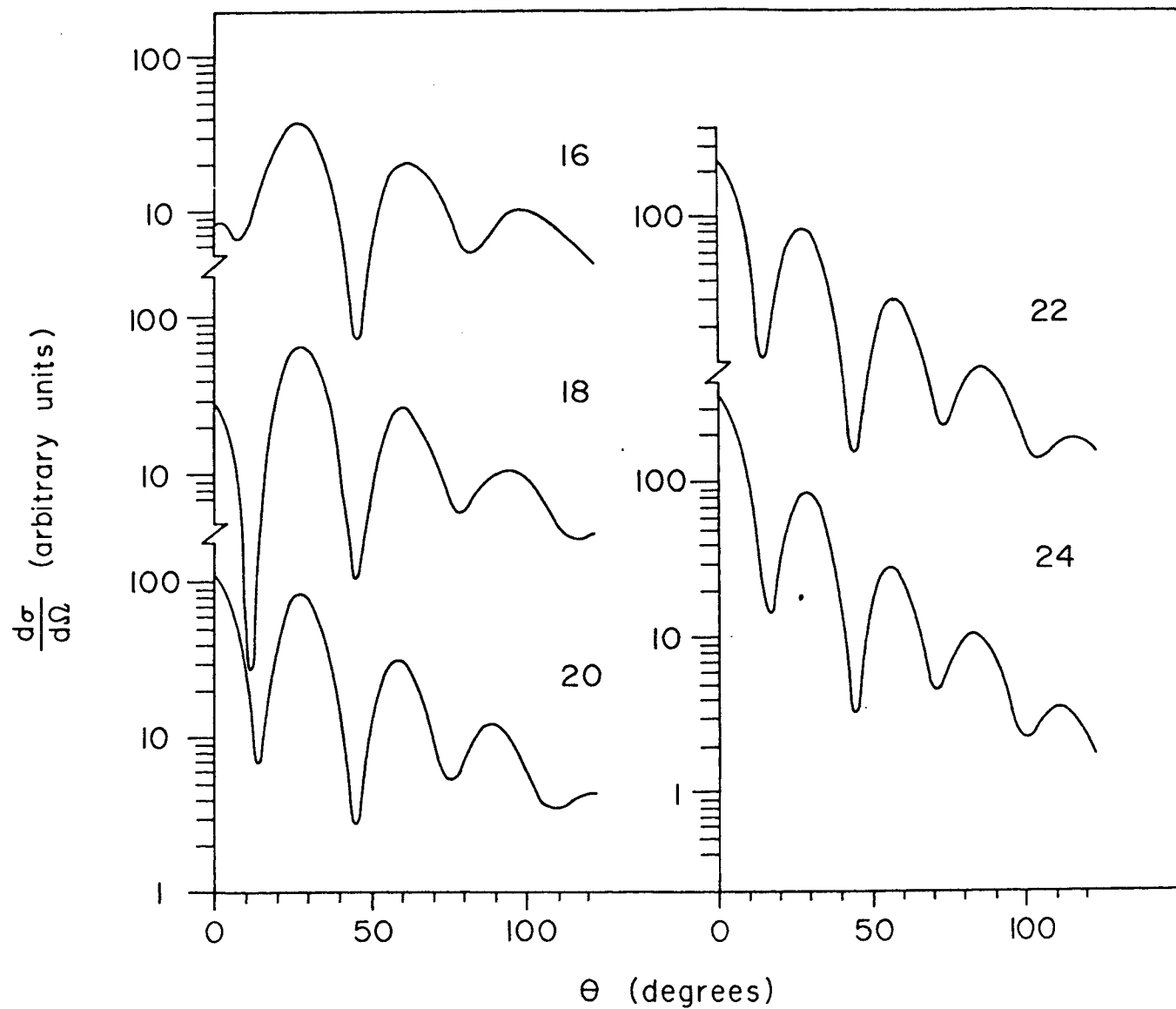


Fig. A1.2 DWBA predicted angular distributions for $l=0$ transitions from the $1h_{9/2}$ state in the $^{151}\text{Sm}(p,t)$ reaction, for different beam energies.

show not only strong $\ell=0$ transitions but also weaker $\ell=2$ and $\ell=4$ transitions, DWBA calculations were performed for $\ell=2$ and $\ell=4$ transitions in the $^{151}\text{Sm}(p,t)$ reaction, for the transfer of a pair of neutrons from either the $1h_{9/2}$ or $2f_{7/2}$ neutron shell. The results of these calculations are shown in Fig. A1.3. Only the angular distribution of the ground state to ground state transition, which resembled that calculated for the $\ell=2$ transfer of a $1h_{9/2}$ neutron pair, was well reproduced by any of the curves shown. It should be noted that the $\ell=2$ angular distribution is 180° out of phase with the $\ell=0$ angular distribution.

It is perhaps rather surprising at first glance, that the DWBA calculations reproduce the experimental data at all, since several rather serious approximations have been made in the calculations. The theoretical calculations assume that:

- 1) the nuclear force is a zero range force, purely local in nature,
- 2) the neutron pair is removed from a single well-defined shell-model state,
- 3) a spherical potential and hence spherical form factor describes the target nucleus,
- 4) the optical model parameters used by Fleming et al. (1970) are reasonable values for samarium, and
- 5) the reaction is a direct single-step process with no channel coupling.

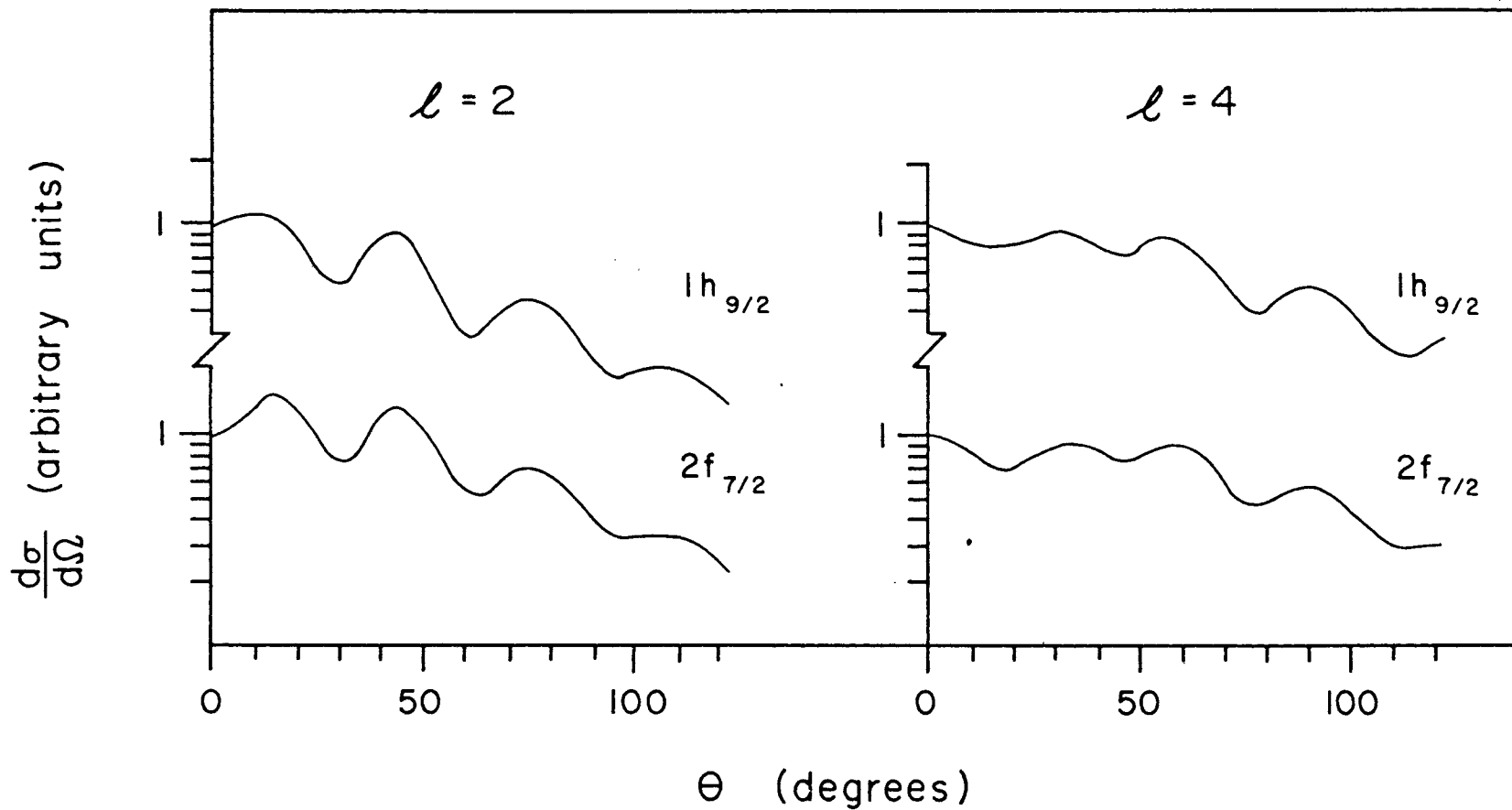
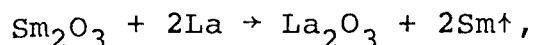


Fig. A1.3 DWBA predictions of $l=2$ and $l=4$ angular distributions for the $1h_{9/2}$ and $2f_{7/2}$ neutron shells.

The fact that the theoretical curves do fit the experimental data relatively well suggests that either the approximations made in the calculations are reasonable or the experiment is rather insensitive to these approximations.

Appendix A2: ^{151}Sm Target Construction

In order to prepare targets of radioactive ^{151}Sm for the experiment, samarium oxide enriched to 93.1% in ^{151}Sm was purchased from the Isotope Sales Division of the Oak Ridge National Laboratory. The isotopic impurities quoted by the supplier were 0.937% ^{147}Sm , 0.041% ^{148}Sm , 0.166% ^{149}Sm , 3.090% ^{150}Sm , 2.390% ^{152}Sm , and 0.263% ^{154}Sm . The oxide was reduced with lanthanum metal using a procedure similar to that outlined by Westgaard and Bjørnholm (1966). At about 1200°C, the vapour pressure of the free samarium generated by the chemical reaction,



is sufficiently great that the samarium may be collected on a target backing above the crucible. However, the vapour pressure of lanthanum is appreciably less than that of samarium at this temperature and consequently only a small amount of lanthanum is evaporated onto the backing.

The carbon backings for the ^{151}Sm targets were prepared using $\sim 50\mu\text{g}/\text{cm}^2$ carbon foils purchased from the Yissum Research Development Company. Since the foils were attached to glass slides with a soluble adhesive, the carbon film could be floated off by gently immersing the slide at a shallow angle in a bowl of distilled water. An aluminum target frame, 1" square with a 3/8" hole in the centre, which was slotted specifically to hold the foil was then used to

to pick up the foil such that the foil would be folded, making it $100\mu\text{g}/\text{cm}^2$ thick in the centre. It had previously been determined that thinner foils were not strong enough to withstand the heat generated in the evaporator used for this work.

Since ^{151}Sm is radioactive via β -decay with a half-life of about 90 years, the entire evaporation procedure was conducted in a glove box in a radiation laboratory. This glove box had been previously outfitted with an evaporator and vacuum system essential to the preparation of the target. Reduction and evaporation occurred in a small tantalum crucible, 1" long and $1/8$ " in diameter, which had a $1/16$ " diameter hole drilled through the centre to contain the mixture of samarium oxide and lanthanum. Heating of the crucible was achieved by passing a high current through it.

Prior to the evaporation of ^{151}Sm , several trial runs were performed using an inexpensive sample of samarium oxide, enriched in ^{152}Sm , to determine the experimental conditions which produced the best targets. There was, however, one unfortunate effect of the trial runs using ^{152}Sm . Although the crucible was cleaned and purged at about 1500°C for 20 minutes before using the samarium oxide enriched in ^{151}Sm , (d,d') reactions performed on the ^{151}Sm target used for this work indicated a concentration of ^{152}Sm in the target which was about 3 times that stated by the

supplier*. This suggests that a new crucible should be used if the isotopic composition for a sample of samarium oxide is different from that previously used.

The procedure used for the construction of ^{151}Sm targets was similar to that used during the trial runs. About 2.5 mg of samarium oxide enriched in ^{151}Sm was "intimately" mixed with ~ 3.5 mg of fresh lanthanum filings. The mixture was loaded into the tantalum crucible and gently packed in. The aluminum frame supporting the $100\mu\text{g}/\text{cm}^2$ carbon foil was mounted about 1.5 cm above the top of the crucible. To shield the foil from some of the heat generated in the evaporation, a tungsten plate with a $1/8$ " hole in it was positioned between the crucible and foil such that only the mouth of the crucible could be "seen" by the foil. The evaporation chamber was then closed and the system was evacuated to $\sim 10^{-4}$ torr. Heating of the crucible was conducted slowly up to about 400°C . If this was not done, gases trapped in the mixture escaped explosively blowing the load out of the crucible. The current was then rapidly increased until the temperature was roughly 1200°C . After heating at this temperature for about 7 minutes, the current was turned off and the crucible was allowed to cool.

The targets produced by this procedure were films of

* The additional concentration of ^{152}Sm is taken into account in the composition quoted in Table 3.1.

samarium approximately $60\mu\text{g}/\text{cm}^2$ thick and about 5 mm in diameter. To guard against radioactive contamination in the event of target breakage, the targets were mounted in a special container (a modified Ingersoll Cheese Spread jar) which could be placed directly into the spectrograph target chamber. The bottom of the jar was then removed, exposing the target. The chamber, which had been previously lined with aluminum foil, was pumped down and the spectra were taken.

The targets of ^{152}Sm and ^{149}Sm had been made previously using a similar technique to that employed in the production of the ^{151}Sm target; however, the difficulties of handling a radioactive material were, of course, not present with the stable isotopes.

References

- Austern, N. 1970. Direct Nuclear Reaction Theories (John Wiley and Sons Inc., New York).
- Bjerregaard, J.H., Hansen, O., Nathan, O., and Hinds, S. 1966. Nucl. Phys. 86, 145.
- Broglia, R.A., Hansen, O., and Riedel, C. 1972. To be published.
- Bunker, M.E., and Reich, C.W. 1971. Rev. Mod. Phys. 43, 348.
- Burke, D.G., Waddington, J.C., and Hansen, O. 1972. Unpublished data. (Work on $^{149}\text{Sm}(t,p)$)
- Chapman, R., McLatchie, W., and Kitching, J.E. 1972. Nucl. Phys. A, 186, 603.
- Elze, W., Boyno, J.S., and Huizenga, J.R. 1972. Nucl. Phys. A, 187, 473.
- Fleming, D.G., Blann, M., Fulbright, H.W., and Robbins, J.A. 1970. Nucl. Phys. A, 157, 1.
- Fleming, D.G., Gunther, C., Hagemann, G.B., Herskind, B., and Tjøm, P.O. 1971. Phys. Rev. Lett. 27, 1235.
- Glendenning, N.K. 1965. Phys. Rev. 137, B102.
- Lederer, C.M., Hollander, J.M., and Perlman, I. 1967. Table of Isotopes, 6th ed. (John Wiley and Sons Inc., New York).
- Maxwell, J.R., Reynolds, G.M., and Hintz, N.M. 1966. Phys. Rev. 151, 1000.
- McLatchie, W., Darcey, W., and Kitching, J.E. 1970. Nucl. Phys. A, 159, 615.
- Meredith, J.O., and Barber, R.C. 1972. Can. J. Phys. 50, 1195.
- Nelson, D.E., Burke, D.G., Cook, W.B., and Waddington, J.C. 1971. Can. J. Phys. 49, 3166.
- Nilsson, S.G. 1955. Mat. Fys. Medd. Dan. Vid. Selsk. 29, No. 16.
- Preston, M.A. 1962. Physics of the Nucleus (Addison-Wesley Publishing Company Inc., Reading, Mass.).
- Robertson, R.G.H., Choh, S.H., Summers-Gill, R.G., and Stager, C.V. 1971. Can. J. Phys. 49, 766.

Spencer, J.E., and Enge, H.E. 1967. Nucl. Instrum. Methods, 49, 181.

Westgaard, L., and Bjørnholm, S. 1966. Nucl. Instrum. Methods, 42, 77.

Yoshida, S. 1962. Nucl. Phys. 33, 685.